Chair of Reservoir Engineering

Master's Thesis

CO_2 Trapping Potential of Reservoir Rocks by Digital Rock Physics

Rene Ritter, BSc

September 2023

MONTANUNIVERSITÄT LEOBEN
www.unileoben.ac.at

AFFIDAVIT

I declare on oath that I wrote this thesis independently, did not use other than the specified sources and aids, and did not otherwise use any unauthorized aids.

I declare that I have read, understood, and complied with the guidelines of the senate of the Montanuniversität Leoben for "Good Scientific Practice".

Furthermore, I declare that the electronic and printed version of the submitted thesis are identical, both, formally and with regard to content.

Date 19.09.2023

Rene Ritter

Signature Author

Rene Ritter

Rene Ritter

Master Thesis 2023

Petroleum Engineering

CO_2 Trapping Potential of Reservoir Rocks by Digital Rock Physics

Supervisor: Univ.-Prof. Dipl.-Phys. Dr.habil. Holger Ott

Co-supervisor/Advisor: Dipl.-Ing. Bianca Brandstätter

Chair of Reservoir Engineering

dpe

MONTAN UNIVERSITÄT LEOBEN

Acknowledgments

I wish to express my sincere gratitude to Prof. Holger Ott and Dipl.-Ing. Bianca Brandstätter. My master's thesis has benefited much from their exceptional mentoring, persistent support, and belief in me. I am incredibly grateful for the opportunity to participate in scientific research, as these opportunities have greatly benefited my personal development.

To my wife, Kristen, you have been my rock. Your understanding, patience, and encouragement have been invaluable to me. Thank you for standing by my side and always believing in me, even during the most challenging times.

I want to express my heartfelt gratitude to my family for their unwavering love, support, and encouragement throughout this journey. Your belief in me has been a constant source of strength, and I am deeply thankful for all the sacrifices you have made to help me pursue my academic goals.

Finally, I want to thank my friend Boris for the countless thought-provoking discussions and insightful perspectives. Your input and feedback have enriched my work and contributed to shaping my ideas in meaningful ways.

Abstract

Carbon Capture and Storage (CCS) refers to a chain of technologies to capture CO_2 from industrial processes. It is possible to store carbon dioxide on an industrial scale and significantly lower greenhouse gas emissions. A thorough understanding of reservoir characteristics and trapping mechanisms is essential to ensure practical application and the highest level of storage safety. Routine and Special Core Analysis (SCAL) programs evaluate fluid-fluid and rock-fluid characteristics and offer insights into displacement and trapping efficiency. However, SCAL studies require a lot of time and resources. Improvements in imaging methods and processing capacity in Digital Rock Physics (DRP) have made it possible to simulate elementary two-phase-flow processes promptly while accounting for differences in reservoir characteristics. Computing various fluid-fluid and rock-fluid combinations effectively by calibrating the simulations using experimental data is possible. This thesis aims to demonstrate how the Morphological Method (MM) can extract trapping curves. We intend to provide essential insights into the viability and efficiency of CCS as a carbon dioxide storage option by utilizing DRP and computational modeling.

The GeoDict simulation tool, mainly the Satudict module, is used to conduct simulations. We use the morphological approach to model drainage and imbibition processes previously developed by the department. The modified MM is applied to assess the capillary trapping potential of CO_2 in reservoir rocks. A particular focus is on analyzing the influence of the Contact Angle (CA) distribution on capillary trapping curves. This curve describes the reservoir rocks capillary CO_2 trapping potential and is crucial for simulating fluid dynamics and storage safety. Various methods to distribute Contact Angles were explored, and numerical results were compared with experimental data from the literature.

To realistically describe capillary trapping curves, it is necessary to identify and investigate the representative elementary volume. The effects of numerical boundary conditions, especially the influence of the numerical Capillary End Effect (CCE), were investigated, and a strategy to mitigate it was developed. Additionally, we varied contact angles and simulated different wetting properties to study the shift from spontaneous to forced CO_2 displacement. The author showed that the morphological method offers valuable insights into CO_2 trapping in reservoirs. They also demonstrated the reliable modeling of capillary end effects at the pore scale.

Zusammenfassung

Carbon Capture and Storage (CCS) bezieht sich auf eine Reihe von Technologien zur Erfassung und Speicherung von CO_2 aus industriellen Prozessen. Es ist möglich, Kohlendioxid in industriellem Maßstab zu speichern und Treibhausgasemissionen erheblich zu reduzieren. Ein gutes Verständnis der Eigenschaften der Lagerstätte und der Mechanismen zur Kohlenstoffbindung ist unerlässlich, um eine praktische Anwendung und das höchste Maß an Speichersicherheit sicherzustellen. Regelmäßige und spezielle Kernanalysen (Special Core Analysis), die Flüssigkeits-Flüssigkeits- und Gesteins-Flüssigkeits-Eigenschaften bewerten und Einblicke in die Verdrängungs- und Kapillareinschlusspotentiale zu bieten, werden häufig verwendet, um diese Informationen zu sammeln. SCAL-Studien erfordern viel Zeit und Ressourcen. In den letzten Jahren haben Verbesserungen in Bildgebungsmethoden und Verarbeitungskapazitäten in der Digitalen Gesteinsphysik (Digital Rock Physics) es ermöglicht, elementare Zweiphasenflussprozesse prompt zu simulieren. Unterschiede in den Lagerstätteneigenschaften werden berücksichtigt. Es ist möglich, verschiedene Flüssigkeits-Flüssigkeits- und Gesteins-Flüssigkeits-Kombinationen effektiv zu berechnen, indem man die Simulationen anhand von Literatur kalibriert. Diese Arbeit soll demonstrieren, wie die morphologische Methode „Capillary Trapping Curves“ extrahieren kann. Es ist beabsichtigt, wichtige Erkenntnisse zur Machbarkeit und Effizienz von CCS als Kohlendioxidspeicheroption unter Verwendung von DRP und Computermodellierung bereitzustellen.

Dazu wird das GeoDict-Simulationstool, insbesondere das Satudict-Modul verwendet, um Drainage- und Imbibitionsprozesse basierend auf dem zuvor am Lehrstuhl entwickelten morphologischen Ansatz zu modellieren. Die modifizierte morphologische Methode wird hierbei auf das Kapillareinschlusspotential von CO2 in Lagerstättengesteinen angewandt. Dabei soll insbesondere der Einfluss der Kontanktwinkelverteilung auf die „capillary trapping cuve“ untersucht werden, die den Zusammenhang von initialer zu residualen CO_2 Sättigung beschreibt..Diese beschreibt das kapillare CO2-Bindungspotential des Lagerstättengesteines und ist für die Simulation der Fluiddynamik und der Speichersicherheit ausschlaggebend. Dazu wurden unterschiedliche Methoden zur Verteilung von Kontaktwinkeln untersucht und numerische Resultate mit experimentellen Daten aus der Literatur verglichen.

Um „Capillary Trapping Curves“ realistisch beschrieben zu können, ist es notwendig, Aussagen über representative Simulationsolumina zu machen. Die Auswirkungen numerischer

Randbedingungen, insbesondere der Einfluss des numerischen kapillaren Endeffekts wurden untersucht und eine Strategie zur Vermeidung entwickelt. Des Weiteren wurden Kontaktwinkel variiert und unterschiedliche Benetzungseigenschaften simuliert, um den Übergang von spontaner zu erzwungener CO_2 Verdrängung zu modellieren. Der Autor hat gezeigt, dass die Anwendung der morphologischen Methode wertvolle Einblicke in die kapillare Bindung von CO2 in Lagerstätten bietet und kapillare Endeffekte auf der Porenskala zuverlässig modellierbar sind.

Table of Contents

Chapter 1

Introduction

Anthropogenic activities, such as burning fossil fuels or deforestation, significantly raise carbon dioxide emissions. CO_2 is a primary greenhouse gas contributing to as much as 70% of the global warming trend. Keeping CO_2 in subsurface geological formations, including deep saline aquifers, active and exhausted oil and gas fields, deep coal seams which are not mineable is one way to address this global problem. Since depleted hydrocarbon reservoirs are deep enough to safely store CO_2 without compromising subsurface resources, they are considered the most appealing choice for long-term, secure, and cost-effective CO_2 storage. Furthermore, they have long-term conserved oil and gas under high pressures and temperatures, which can lessen the risk of leaking during long-term storage. Four trapping mechanisms—structural and stratigraphic trapping, capillary trapping, solubility trapping, and mineral trapping—can occur when CO_2 is delivered into a storage medium. Although capillary trapping is the most effective method for quickly entrapping CO_2, it is frequently disregarded when considering depleted hydrocarbon storage media. However, few studies have investigated the effect of capillary trapping to estimate residual CO_2 saturation (Raza et al. 2016).

Researchers constantly look for new and creative ways to examine the characteristics of reservoir rocks and assess their potential for CO_2 storage. DRP, a method that has gained popularity, offers a formidable tool for investigating the characteristics of rocks and assessing the potential for CO_2 storage in oil reservoirs.

The capillary trapping potential of rock samples largely determines the efficacy of CO_2 storage in oil reservoirs. Traditionally, this evaluation required physically measuring the samples in a lab, which might be expensive and time-consuming. DRP offers a more cost- and time-efficient method to deliver more precise results faster.

To simulate various physical processes, such as the fluid flow through porous media, DRP creates a three-dimensional representation of the rock sample, which is called digital twin. One

can assess the rock's capillary trapping capability and determine how much CO_2 can be trapped in the rock matrix by simulating the flow of fluids through a rock sample.

One of the critical benefits of DRP is that it enables scientists to analyze a wider variety of rock samples in a shorter period. As a result, it will be possible to conduct a more thorough investigation of rock characteristics and CO_2 storage capability, enabling better-informed decisions to be made about the viability of CO_2 storage in reservoirs (Dvorkin et al. 2008).

The ability to evaluate rock qualities in a broader range of situations, such as various pressures and temperatures, is another benefit of DRP. This gives a thorough understanding of the possibilities for CO_2 storage and can assist in locating the reservoir locations that offer the best chances for storage.

DRP is an innovative method for analyzing the characteristics of rocks and assessing the potential for CO_2 storage in oil reserves. DRP has the potential to completely change how we approach energy exploration and CO_2 storage thanks to its capacity to deliver precise and thorough data more effectively and economically.

1.1 Background and Context

The Morphological Method is a technique that applies morphological operations to pore-scale rock images using mathematical principles developed by Matheron and Serra in 1964 (Georges Matheron and Jean Serra 1998). The technique uses dilation and erosion operations on the rock's structure to identify pore throats or drainage displacement thresholds. This enables quantitative analysis of pore geometries and links them to capillarity and fluid displacement physics.

By means of the MM, the distributions of wetting and non-wetting phases inside a porous medium assume capillary forces dominate over viscous forces. It uses morphological operations to distribute the two fluid phases and describes displacements at low capillary numbers. The technique changes the topology of the fluid phases and corresponds to the physical event of a capillary pressure change. The number of dilated voxels describes the pore throat size in drainage. The Schulz method introduces different contact angles, which scale the dilation radius with $\cos(\theta)$. Still, this method is unsuitable for contact angles close to 90 degrees (Schulz et al. 2015).

Primary drainage is the displacement of the Wetting Phase (WP) by the Non-Wetting Phase (NWP). It is followed by the imbibition process, which is the displacement of the NWP by the WP. Imbibition can have positive and negative capillary pressures at different saturation ranges. Positive capillary pressure indicates a spontaneous process, and negative capillary pressure

indicates a forced process. Therefore, the Spontaneous Imbibition (SI) process must be coupled with a subsequent forced process to simulate the full imbibition range with the MM. The transition period from spontaneous to Forced Imbibition (FI) happens when the capillary pressure reaches zero. This is implemented by introducing non-wetting material before the start of the spontaneous imbibition modeling through a stochastic field introduced before or after the drainage process.

1.2 Scope and Objectives

The influence of forced imbibition has consistently posed challenges in simulating hysteresis phenomena. In response to this challenge, our objective was to effectively incorporate a methodology that enables the comprehensive simulation of the entire spectrum of these processes. Since the microscopic effects are still not fully understood, we used stochastic and deterministic approaches to get a better understanding.

The stochastic method was explicitly adopted to explore how forced imbibition impacts the capillary trapping potential. This approach was chosen to introduce randomness and variability into the analysis, allowing us to understand the nuanced effects of forced imbibition on trapping behavior.

This study systematically investigates various scenarios using the appropriate domain size and boundary conditions. We must note that our focus is solely on systems that exhibit purely water-wet behavior, which will not be altered. However, by introducing non-wetting material, we can influence the ratio of spontaneous to forced imbibition by accurately simulating advancing and receding contact angles during imbibition. This is because the distribution of wetting material can affect the medium's relative permeability and capillary pressure curves, which are essential to predict the behavior of the fluid phases in the experimental setup.

We align our simulations with the experimental range to benchmark them effectively. We aim to establish a consistent range and experimental conditions fitting into the benchmark of experimental data from the literature. The simulations were performed on a digital twin of a Berea sandstone, due to the widely available literature data.

Chapter 2

Literature Review

One must understand the workflow, methods, analytical tools, and computational methodologies to better understand the technical aspects of capillary trapping curves and hysteresis. The motivation for this study comes from the pore physics aspect of the carbon capture and storage (CCS) process. The relationship between pore size distribution and capillary pressure saturation during drainage and imbibition processes forms the basis of this work. This physical principle allows us to capture hysteresis in capillary saturation relationships. Furthermore, it allows us to apply this method in the form of morphological methods on a digital twin. In the following steps, the Land Model is used to compare the results of this study and compare them with the literature.

2.1 Carbon Capture and Storage

The climate system has undergone extraordinary changes, which have caused a notable rise in surface temperature over the last few decades. Carbon dioxide, methane, and nitrous oxide are only a few greenhouse gases that have been steadily released into the atmosphere due to industrial processes, transportation, agriculture, and deforestation. Several strategies have been implemented to address the rising CO_2 levels in the atmosphere, including cutting back on energy use, switching to fuels with shorter carbon chains, and capturing and storing CO_2. By injecting CO_2 into geological formations, CCS technology has shown promise in lowering CO_2 concentrations. (Krevor et al. 2015). By 2100, CO_2 levels in the atmosphere might be reduced by successfully adopting CCS to 450 ppm. The notion of CCS was first developed when it was proposed that CO_2 from coal power stations could be captured and injected into suitable geological formations. (C. Marchetti 1977).

To cut global CO_2 emissions by 17% by 2050, the International Energy Agency has advised CCS implementation in every nation. According to S. BACHU and J. SHAW, some 800

sedimentary basins worldwide are ideal geological sites for CO_2 storage. Several CCS initiatives have started in recent years as a result and are shown in Figure 1. Among the innovative CCS projects are In-Salah in Algeria and Sleipner in Norway. Sleipner began injecting CO_2 into a saline aquifer with a 0.9 million ton per year (MMt/yr) capacity in 1996. An industrial-scale demonstration project called In-Salah was started in Algeria to examine whether injecting CO_2 into an aquifer with a 1.2 Mt/year capacity was feasible (Alexander 2016). Shell runs the CO_2SINK project in Germany, which aims to monitor and inject CO_2 into a deep onshore saline aquifer. As the first demonstration project to examine the economic and technological viability of storing CO_2 in coal seams, Reduction of CO_2 Emission utilizing CO_2 storage in coal seams (RECOPOL) is a pilot project to reduce CO_2 emissions by storing CO_2 in Poland's Silesian Coal Basin coal seams. Many CCS projects have been carried out throughout the last few decades (Raza et al. 2019).

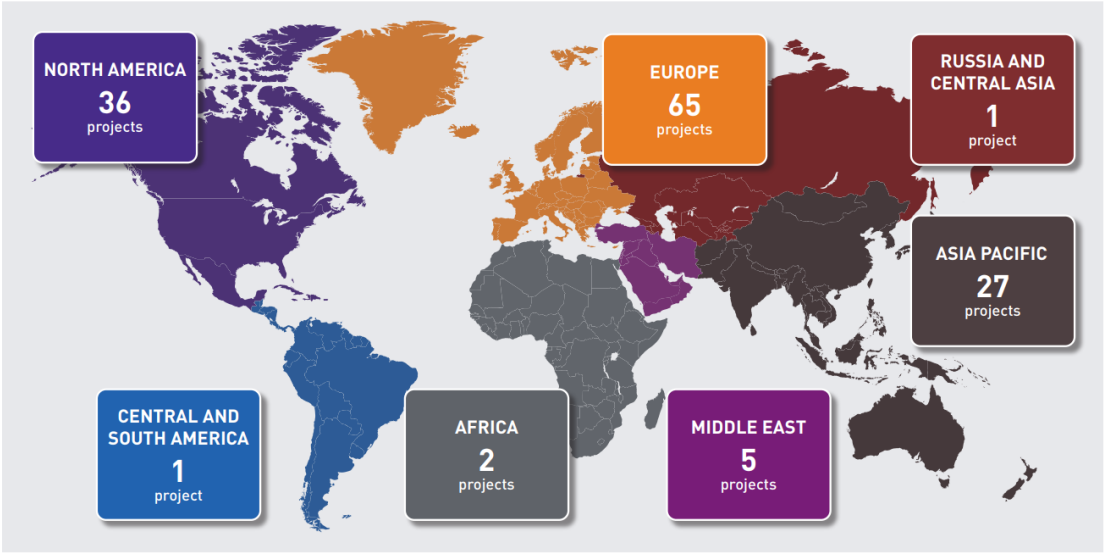

Figure 1: Summarizes the present and future CCS sites worldwide as of April 2021 (IOGP Publications library 2023).

2.1.1 Capture Options

Changing or reengineering an existing industrial process to produce a stream of CO_2 that is pure or almost pure is one of three main approaches for capturing CO_2. This can be done by employing oxy-fueling, chemical looping power plants, and pre-combustion fuel gasification. Another choice is to concentrate industrial-process emissions to create a stream that primarily contains CO_2. Post-combustion gases from cement or power plants can be separated to do this. A stream of pure CO_2 or a chemically stable product is produced when CO_2 is directly separated from the air. The mineralization of steel slag serves as one example of this.

2.1.2 Storage Options

Geological storage

Injecting CO_2 into geological formations like oil, gas, and water-bearing ones is the most promising method for large-scale CO_2 storage. Oil and gas reservoirs offer economic benefits and can be used for Enhanced Oil Recovery (EOR). However, saline aquifers have much greater storage potential. Global estimates show there is sufficient capacity for CO_2 storage. Saline aquifer storage is highly accessible and can store much more CO_2 than oil and gas reservoirs. Numerous projects worldwide are planned to store CO_2 in oil and gas reservoirs and saline aquifers. Technologies for site characterization, injection, and monitoring for geological storage are also being developed (Stephen A. Rackley 2017).

Ocean Storage

Includes directly dissolving CO_2 into deep waters or storing it as a supercritical fluid lake beneath the seabed. However, these options face environmental opposition, limiting their progress. Other approaches involve enhancing natural carbon sequestration processes through fertilizing surface waters or mimicking the weathering of rocks in the ocean. These methods need wide dispersal to avoid local environmental impacts (Stephen A. Rackley 2017).

Storage in terrestrial ecosystems

Terrestrial ecosystems serve as carbon sinks through various organic products with different lifetimes. Enhancing carbon storage involves directing carbon into longer-lived pools, achieved through land use, management practices, plant types, and soil conditions. The increased carbon flux from the atmosphere to terrestrial ecosystems partially offsets human carbon emissions due to higher CO_2 levels and climate changes. Another option for carbon storage is producing biochar through biomass pyrolysis and storing it (Stephen A. Rackley 2017; Jayasekara et al. 2020).

Mineral carbonation

Mineral carbonation is a promising carbon storage method involving reacting naturally occurring oxides or silicates with CO_2 to form stable carbonates for storage. While it requires large-scale mining and disposal operations, using alkaline waste from industries can offer smaller-scale applications with economic incentives. Mineral carbonation is suitable for dispersed, smaller industrial sources or where CO_2 transportation and local geological storage are challenging. However, further research is needed to optimize the process and assess its long-term viability and environmental impacts (Sandra Ó. Snæbjörnsdóttir et al. 2020).

Other options

Ninety million tons of industrially produced CO_2 are consumed annually as a feedstock for urea manufacturing. Methanol, polyurethanes, and food are also made from it, but they are not appropriate for long-term storage because they have a limited carbon retention period. The production of precipitated calcium carbonate for the paper and cement industries, using cooled flue gases as a source of CO_2 for microalgal photosynthesis, and using catalytic processes to transform CO_2 into fuels like methane and methanol are additional potential uses that could have a significant impact.

2.1.3 CO_2 Injection

There are three options to differentiate between carbon CCS options: Super Critical (SC) CO_2 storage, Carbonated Water Injection (CWI), and CO_2 storage in foams. These options are considered mature enough for potential use in a commercial-scale CCS project. The options are evaluated based on storage capacity, security, and injection rates, and the disadvantages and advantages of each technique are presented.

Supercritical CO_2 Injection

Once captured, the CO_2 is injected into underground formations that are deep enough, typically at least 800 meters, to allow the CO_2 to reach its supercritical state (T = 31.04 °C, P = 73.82 bar) (Ott and Oedai 2015). This results in two phases: the supercritical CO_2, which makes up the majority and forms a "plume," and the aqueous CO_2, which is dissolved in brine. The solubility of CO_2 in water increases as it reaches the supercritical state, but it remains low, so most of the injected CO_2 will remain in the plume. However, the supercritical state does have benefits, as CO_2 behaves like a liquid but flows like a gas (Ott and Oedai 2015). This is due to its increased density, which allows it to store a large amount of mass per volume of pore space. To ensure permanent storage of the CO_2 within the reservoir, a low-permeability formation of a "cap rock" at the top of the reservoir is needed to prevent CO_2 from migrating upwards (Celia et al. 2015). One of the main concerns with CCS is the potential leakage and migration of CO_2, brine, or both to shallower depths, drinking water aquifers, or even the surface (Celia et al. 2015).

Three methods can be used to reduce the need for a tight seal when storing CO_2 underground: capillary entrapment, water dissolution, and mineralization. Mineralization is considered the safest option because a chemical reaction between CO_2 and the rock surface forms a solid carbonate, effectively trapping the CO2 in an immobile secondary phase for thousands to millions of years. Capillary entrapment, also known as residual entrapment, occurs when the injected CO_2 displaces liquid in the formation, causing the remaining CO_2 to become trapped

in the pores due to capillary forces. This is mainly discussed in this work. Another option is dissolution in water, where the water acts as a carrier for the CO_2 and transports it down due to density differences. The solubility of CO_2 in water decreases with increasing temperature and salinity. Lastly, structural or stratigraphic trapping, which relies entirely on an impermeable overburden, can also be used (Liao et al. 2020).

The low viscosity of CO_2 makes it highly mobile, which can lead to low sweep efficiencies during injection into a reservoir. Simultaneous Water and Gas injection (SWAG) or Water Alternating Gas injection (WAG) can increase CO_2 sweep efficiency to address this issue. These methods reduce the mobility of CO_2 and improve sweep efficiency in experimental studies. However, it is worth noting that large amounts of water injected can also reduce the total storage capacity (Lyu et al. 2021).

When CO_2 is initially injected into a reservoir, the active capture mechanisms are mainly hydrodynamic and structural. Over time, the previously discussed long-term capture mechanisms also come into play. One of the main challenges is to increase the low sweep efficiency caused by the low viscosity and density of injected CO_2. (L. Nghiem et al.) suggest adjusting the injector's location and rate, which can increase the amount of retained and dissolved CO_2 by placing the brine injection well above that of the CO_2 injection. Hassanzadeh et al. also proposed accelerating CO_2 dissolution by injecting brine into the CO_2 injector. Shariatipour et al. also presented a method of extracting brine from the top of the aquifer, mixing it with CO_2 through a downhole mixer, and then injecting the dissolved CO_2 back into the same formation. The high water pressure favors the solubility of CO_2 in water. Capillary pressure influences the migration of the CO_2 plume, showing that capillary pressure increases in the post-injection phase but has little impact during the injection itself (Abbaszadeh et al. 2020).

According to Jayasekara et al. (Jayasekara et al. 2020), the integrity of the overburden can be affected when supercritical CO_2 is injected into deep saline aquifers. They found that the dissolution of the caprock mineral is significant in high ionic strength pore liquid compared to low ionic strength liquid. Additionally, when high saline fluid flow is present, the permeability of the overburden can be reduced due to the evaporation of water in the supercritical CO_2 phase, resulting in a brine that is supersaturated with salts. As a result, they propose that aquifers containing high-salinity brine should be selected for CO_2 sequestration to ensure the overburden's long-term integrity, as the permeability and porosity reduction when the SC-CO_2 flux is advection-dominated.

Carbonated Water Injection

Carbon Water Injection (CWI) is a CO_2-EOR method that aims to improve sweep efficiency by evenly distributing CO_2 in the pore space, leading to a delayed breakthrough time. According to (Esene et al. 2019), CWI has a low CO_2 content of 0.02 to 0.05 molar fraction. While it has been demonstrated that CWI can increase oil recovery, the amount of CO_2 storage is limited. However, (Mohammad Derakshanfar 2012) argues that EOR projects are still considerable for geological CO_2 storage due to the known geology of oil reservoirs and the ability to offset the costs of capturing, transporting, and storing CO_2 through additional oil extraction. However, well construction can also be affected by the injection of CO_2, potentially damaging equipment such as pipes, casing, cement, and downhole equipment.

(Cao et al. 2021) emphasized that the likelihood of buoyancy-induced leakage is low because the higher density of Carbonated Water (CW) compared to brine pushes the liquid down, effectively trapping it over time. Motie and Assareh state that the more CO_2 dissolved in CW, the more oil can be recovered and the more CO_2 trapped in the reservoir. However, it is worth mentioning that the maximum solubility of CO_2 in water (at reservoir conditions) should be considered.

Furthermore, (Motie and Assareh 2020) point out that increasing CW's injection rate negatively impacts CO_2 sequestration. A simulation study by (Mohammad Derakshanfar 2012) pointed out that an increase in the injection pressure of CO_2 leads to a corresponding increase in the CO_2 stored in the reservoir. Despite the undeniable benefits of improved storage security and the ability to store CO_2 even beyond 800m, the highly corrosive nature of CW somewhat detracts from these benefits. However, CWI can provide an alternative for offshore operations as it does not require a large-scale source of CO_2, as only small amounts can be added to the water.

CO_2 Storage in Mafic and Ultramafic Rocks

In addition to CO_2-EOR, CCS projects often involve injecting CO_2 into large sedimentary basins, such as the Sleipner field in Norway. These projects rely on the long-term trapping of minerals in such deposits, which can take tens of thousands of years. Sigurdur R. and Gislason and Eric H. Oelkers note that this is due to the slow reaction speed of silicate minerals and the lack of calcium. To address these limitations, researchers have attempted to inject CO_2 into more reactive rocks, such as basaltic rocks, which contain high levels of calcium, magnesium, and iron oxides and are abundant on the earth's surface. These metals in basaltic rocks can react with the injected CO_2 to form carbonate minerals, thus increasing the efficiency of CO_2 storage.

The CarbFix project in southwest Iceland has demonstrated the feasibility of CO_2 storage by mixing water and CO_2 at a depth of 350m, in contrast to conventional mixing at the surface. According to (Sigurdur R. and Gislason and Eric H. Oelkers 2014), the dissolved CO_2 in water accelerates the release of metals from mafic rock. It forms solid carbonate minerals, with over 80% of injected CO_2 being carbonized within a year at depths of 500-800m. However, it should be noted that significant amounts of water are required, with (Alcorn et al. 2020) stating that 32 tons of fresh water are needed to dissolve each ton of CO_2. This storage method may require more wells to store more CO_2 and promote the reaction of CO_2 with the rock. However, this may not result in higher project costs as drilling beyond 800m is reduced. CCS projects in porous basalts are feasible with seawater and freshwater (Eric H. Oelkers et al. 2020). The mineralization of CO_2 near the wellbore can lead to clogging, so selecting target formations with slower reaction rates may be beneficial for the long-term storage of CO_2.

Foam

Foam injection effectively controls gas mobility in the oil and gas industry and cleans groundwater. In addition to extracting oil, using foam in EOR also allows for the storage of CO_2. A foam is a mixture of gas bubbles (usually CO_2) suspended in a liquid, known as lamellae. This can help decrease the adverse effects of low gas viscosity and decrease relative gas permeability, improving efficiency and reducing the formation of thick fingers. Adding surfactants to the liquid can further stabilize the lamellae.

The storage capacity for CO_2 is increased by increasing the contact area between the rock and the injected CO_2 due to the dispersion of CO_2 in the liquid phase. The area that the CO_2 can reach is also increased due to the decrease in gas mobility (Alcorn et al. 2020).

The high viscosity of foam can lead to the need for additional wells and lower injection rates, which can be a financial obstacle. According to (Lyu et al. 2021), when a fixed injection rate is used, the pressure required for foam is approximately 1.33 times higher than that of SWAG. Foam injection can decrease gas mobility and increase the amount of retained CO_2. However, (Lyu et al. 2021) note that the difference in ultimate SC-CO_2 capture and CO_2 storage in foams may not be significant in the long term. Despite this, foam injection is a valuable method to boost final yield during CO_2 EOR because it can significantly delay breakthroughs and improve sweep efficiency.

Additionally, foam injection can prevent the upward movement of the CO_2 plume due to gravity, thereby increasing storage safety. Foam injection can be applied in CO_2-EOR projects and saline aquifers. The benefits of CO_2-EOR are clear, but the benefits of storage in saline aquifers still need further research. However, improved storage security is another advantage of this technology. The injectivity is also debatable due to the high foam viscosity.

Storage Capacity and Security

Regarding storage options for CO_2, foam and CWI have higher storage security than SC-CO_2 injection. However, the foam has lower injectivity, possibly requiring additional wells for adequate storage. The storage capacity of CWI can vary depending on the operation, with higher capacity possible when mixing occurs on the way down into the reservoir. The storage capacity of SC-CO_2 and foam is equal, as reported in a simulation study by (Lyu et al. 2021). It is worth noting that SC-CO_2 has the lowest storage security as it requires the presence of an impermeable (or at least low-permeability) overburden.

2.2 Trapping Mechanisms

While there are no established performance standards for sequestration projects, it is widely accepted that high retention rates are essential. Large-scale sequestration efforts should aim for 90-99% retention rates over 1000 years, according to (Hepple and Benson 2005). Four trapping mechanisms, visualized in Figure 2, contribute to long-term retention: structural, solubility, capillary, and mineral trapping. As time passes and CO_2 reacts with rocks and fluids, the importance of these mechanisms is expected to shift. Initially, retention will depend mainly on the primary seal, but as secondary immobilizing processes take effect, this dependence will decrease (Benson and Cole 2008).

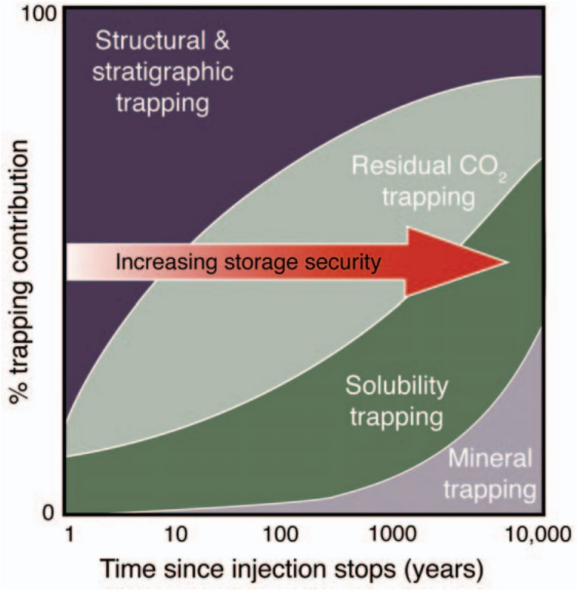

Figure 2: CO_2 capturing mechanisms. Over time, geochemical trapping has replaced physical trapping (IPCC special report on carbon dioxide capture and storage 2005).

The most prominent mechanism is structural trapping, where a thick and fine-textured rock serves as a barrier to prevent upward migration. Capillary trapping occurs when CO_2 injection ceases, and water enters the CO_2 plume, immobilizing the trailing edge and reducing up-dip migration speed. Solubility trapping occurs when CO_2 is dissolved into the pore water, which relies on pressure, temperature, and salinity. As pressure increases, CO_2 solubility increases, but it decreases with an increase in temperature and salinity. Mineral trapping happens when dissolved CO_2 interacts with minerals in the geological formation, leading to the precipitation of carbonate minerals. Mineral trapping, while capable of immobilizing CO_2 for significantly extended periods, is a slow process that may take tens to hundreds of years to have a significant impact.

2.2.1 Capillary Trapping

Initial brine displacement occurs when CO_2 is added to the reservoir during residual capillary trapping. After the injection is discontinued, the CO_2 flows laterally due to viscous forces and upward due to density differences. Thus, the non-wetting phase (CO_2) allows the brine to enter the pores. Following the displacement of the CO_2 by the brine, a significant amount of CO_2 is trapped in tiny clusters of pores (Ajayi et al. 2019). Capillary or residual trapping are two terms used to describe how CO_2 is trapped and becomes immobile (Zhang and Song 2014).

According to (Saadatpoor et al. 2010), CO_2 cannot be transported because of the surface tension between CO_2 and brine, which causes a more considerable capillary entry pressure than rock pressure. As the pores are saturated with residual gas, CO_2 becomes trapped there. The plume leaves behind immobile CO_2 as it rises along an imbibition saturation path, which causes the snap-off and gas trapping (Juanes et al. 2006). This occurrence is more common when there are microcapillary heterogeneities in a rock. According to recent studies, capillary trapping is a short-term CO_2-trapping method that is more effective than other processes (Lamy et al. 2010). It works because capillary forces outweigh buoyant forces, which prevents CO_2 from being confined by a caprock that has been somewhat weakened and instead causes it to appear as pore-scale bubbles.

Furthermore, a considerable percentage of the CO_2 injected is trapped in the hysteresis model due to residual trapping, which severely restricts the mobility of the gas. The storage of CO_2 is significantly impacted by residual gas (Zhang and Song 2014).

2.3 Percolation

The nature of displacement is controlled by two separate processes which compete. Figure 3 visualizes how wet layers swell first, and this causes them to snap off. As a result, the wetting phase surrounds the non-wetting phase in fewer areas, trapping it inside more pronounced

pores. The security of CO_2 storage, the amount of trapped CO_2 close to the water table, and oil recovery are all significantly impacted by this. In the second procedure, nearby pores that have already been wetted advance piston-like to fill holes and throats. Displacement caused by drainage is the opposite of this. We can concentrate on applications in oil recovery and make the topic less abstract if we assume that the wetting phase is water and the non-wetting phase is CO_2. All surfaces will still be regarded to be water-wet with contact angles less than 90° despite taking wettability change and contact angle hysteresis into account (Martin Blunt et al. 1992).

2.3.1 Flow phenomena during percolation

Primary drainage occurs in oil reserves over geological timeframes, resulting in fluid capillary equilibrium. This equilibrium is defined by a constant interfacial curvature between the NWP and the WP in a tiny rock section. This balance holds for the terminal menisci that cross a pore or throat and the arc menisci in the corners and roughness of the pore space. The height above the free water level determines the same capillary pressures at the microscopic and macroscopic scales. Flow rates are high near the well, and the injection pressure is high, but flow rates are often significantly lower in the middle of the reservoir. With a slow rise in water pressure and saturation and a matching decline in capillary pressure, flooding can continue for decades until the saturation has increased over the field (Yu and Wardlaw 1985).

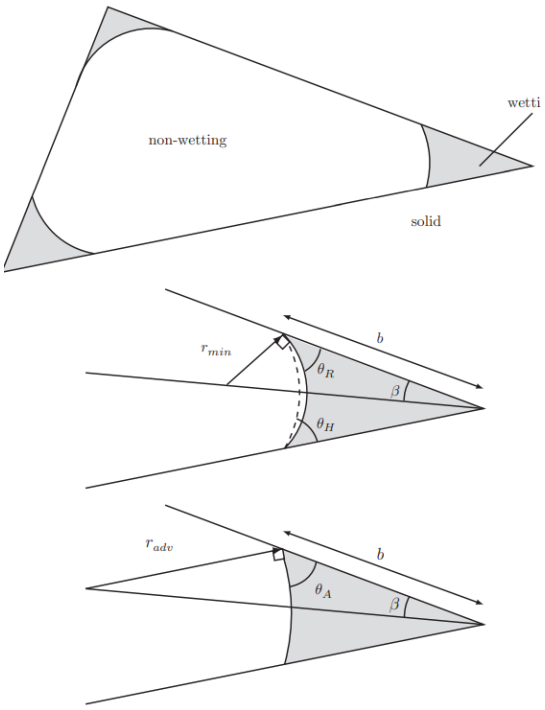

Figure 3: Swelling, Layer Flow and Snap-Off (Blunt 2017)

If the initial capillary pressure is high, the oil fills the bulk of the pore space while the injecting fluid is confined to layers in its corners, rough portions, and some of its tighter regions. As the pressure increases, these layers spread out, allowing the saturation level to grow uniformly throughout the system. When conditions are extreme, and CO_2 is only available in thin layers, water cannot be quickly displaced from a pore that is filled with CO_2 nearby. CO_2 fills the pore space and partially fills the two adjacent pores at the snap-off point when the layers expand to their maximum extent. This mechanism significantly affects both the fluid distributions and the

amount of non-wetting phase. Pictures demonstrate the process, and each displays an idealized portion of pore space with a triangular cross-section.

A pore or throat cross-section taken after primary drainage shows the wetting phase (water) at the corners and the non-wetting phase (CO_2) in the middle. The corner's corner half-angle, receding contact angle, and associated radius of curvature are all visible in a more comprehensive examination of the corner. The first reduction in capillary pressure results in pinned and immobile contact between the solid, water, and CO_2. But when the contact angle rises, so does the radius of curvature. The dotted line shows the interface with a hinging contact angle. Only when the advance contact angle A is reached, and the radius of curvature radii is greater than r_{min}, the contact line begins to move. This process of contact line movement is crucial to the displacement of the non-wetting phase by the wetting phase (Blunt 2017).

2.4 Pore Morphology Method

The Full Morphological Method, often referred to as the Pore Morphology Method, is an approach designed for porous media that is based on the ideas of mathematical morphology in the writings of (Bryant et al. 1993), (Bakke and Øren 1997) and (Hilpert and Miller 2001). The technique uses morphological operators to examine the pore structure of porous media, including dilation, erosion, and opening.

Geometrical operations involving two or more objects are the foundation for the morphological operators, notably Minkowski addition and subtraction. These operators perform dilation and erosion operations on the pore space in the porous media. These operations can be used by the method to determine capillary pressure.

The Young-Laplace equation, which describes variations in capillary pressure, provides the foundation for the capillary pressure calculation. This equation is based on the idea that changes in the radius of curvature of the pore space cause these variations. Figure 4 shows how 3D photos of a sample can be used to determine capillary thresholds and the pore size of a particular porous media using the MM with a spherical object.

Several phases in the initial iteration of the algorithm's process, which is used in Geodict, can apply the Pore Morphology Method (Hilpert and Miller 2001). These procedures aim to investigate the pore structure and quantify capillary pressure using morphological operations.

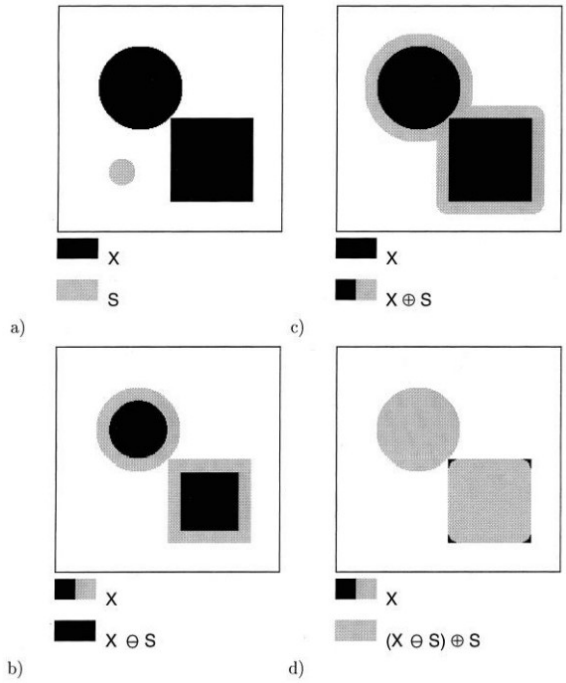

Figure 4: Two-dimensional morphological operations include (Hilpert and Miller 2001)

The reservoir(s) WP is situated on one of the model's boundaries, and the digital porous medium's initial state contains the WP. The NWP phase of the simulation process begins with spherical objects entering the digital porous medium during the NWP phase. As the capillary pressure rises due to the spheres' reducing radius, the intrusion is caused by the eroded WP from rock grains.

As the capillary pressure rises, the invading spheres gradually invade the smaller pores as they fill the bigger pores first. This is how the intrusion process works. Careful control of the morphological procedures is necessary to guarantee that the NWP phase maintains its connection to the NWP reservoir and establishes the appropriate capillary pressure corresponding to the intruding sphere diameter.

Figure 5 provides a visual representation of this process by simulating the entrance of the NWP phase into the porous medium using a series of morphological techniques. Black spheres represent the solid substance. In Figure 5, we see that only the NWP phase in the pore space that is entirely connected to the NWP reservoir is left for this stage in (a), and (b) the solid/NWP interface is reshaped following the planned contact angle in (c) flowing from bottom to top.

With this systematic methodology and the application of morphological operators, the invasion of the NWP phase into various pore sizes and structural configurations inside the digital porous medium may be accurately represented. As a result, the fluid behavior and pore-scale displacement mechanisms in the reservoir rock are thoroughly understood.

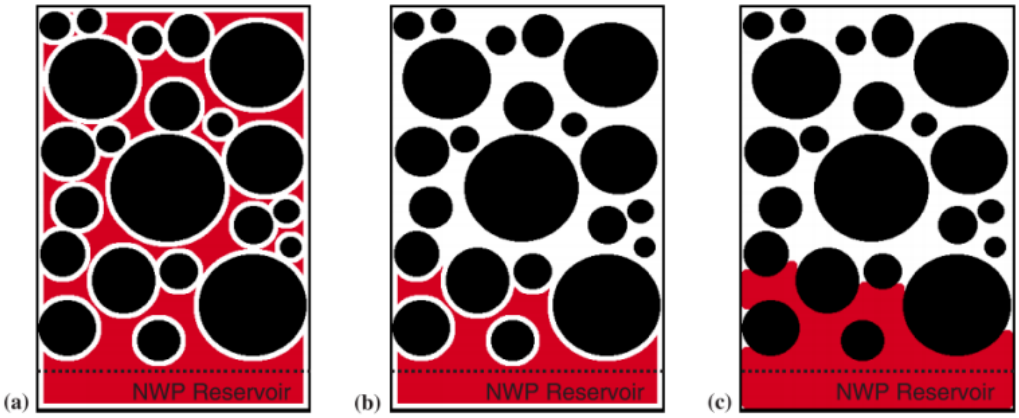

Figure 5: Representation of the drainage simulation's initial 2D picture. (Hilpert and Miller 2001)

Even though the morphological technique utilized in Geodict yields realistic results for drainage simulations, it has certain restrictions regarding modeling imbibition processes. The ganglion dynamical flow mechanisms seen on the continuous scale of rocks are not entirely captured by the morphological technique, which concentrates on the local pore-to-pore scale. These mechanisms include the NWP displacement like a piston, wetting-layer snap-off, rivalry between them, and subsequent trapping of NWP.

Ganglion dynamics are essential in imbibition processes, especially at greater wetting-phase saturations. These mechanisms, which are not expressly considered by the morphological technique, which acts at a more localized level, include the interaction and behavior of fluids at a larger scale than individual pores.

The morphological method produces gratifying results for imbibition simulations, albeit with drawbacks, especially at lower wetting-phase saturations. The approach can accurately reflect the imbibition process in various situations, as demonstrated by comparing tests and simulations.

The current method in use by Geodict for estimating imbibition uses a reverse drainage mechanism. The two phases' contact angles are switched, and the simulation continues until the NWP's residual saturation is attained.

The morphological approach helps comprehend fluid dynamics and displacement processes at the pore scale in porous media, even though it has several drawbacks. Researchers are still investigating and developing Alternative approaches and models to represent better ganglion dynamics and other intricate flow patterns seen at greater scales.

Once the supercritical state is reached, the CO_2-brine experimental settings can have unpredictable results. There have been numerous observations of the effects of variables like temperature, pressure, and salinity. On the other hand, the morphological method primarily

concentrates on the wetting state of the porous medium and does not directly incorporate or rely on these effects.

The morphological approach's limits and scale issues must be understood to be used effectively when examining CO_2 trapping in a porous medium. Researchers should carefully interpret and relate the micro-scale simulation results to the macro-scale experimental observations to gain a thorough understanding of CO_2 trapping mechanisms in actual reservoirs, even though the method offers insightful information into pore-scale fluid behavior and displacement processes.

2.5 Domain Size and the Effect of Capillarity

2.5.1 Representative Elementary Volume

The smallest volume that can be measured to get a value that is reflective of the whole is known as the Representative Elementary Volume (REV) of a uniform porous medium. Bear and Bachmat offered this description in their 1998 paper.

To guarantee that the properties being assessed or modeled faithfully depict the entirety of the rock sample or reservoir. In simpler terms, the goal was to determine the size range of the digital twin within which we can estimate the rock structure's ability to trap capillary fluids. Figure 6 conceptually visualizes the area of a representative elementary volume between the microscopic and the macroscopic domain size.

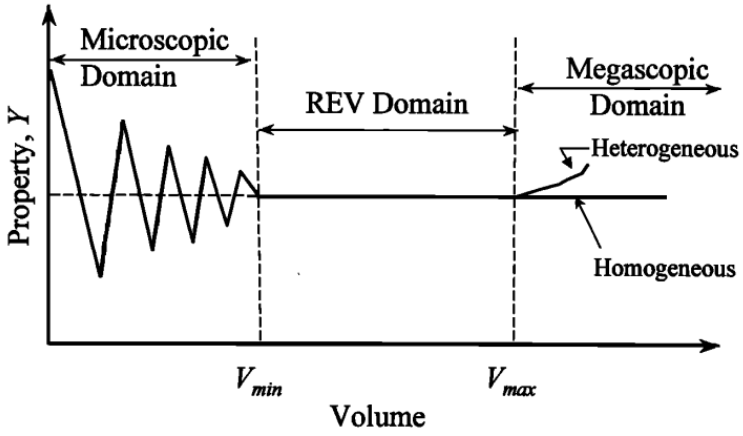

Figure 6: Conceptual visualization of the representative elementary volume (Brown et al. 2000)

Additionally, it plays a crucial function as a perceptive tool for understanding the intrinsic variability in larger samples, providing crucial insights into the characteristics of the rock.

2.5.2 Capillary End Effect and Mirroring

The capillary end effect is a factor when measuring trapping curves during experiments. CEE describes the distortion of fluid retention patterns caused by capillary forces near the outlet of the porous sample. This effect can significantly influence the precision of measurements of the trapping curve, resulting in inaccurate evaluations of the fluid trapping potential. Experimental data may be distorted by capillary end effects, leading to inaccurate trapping curves. These errors impact the sample's spatial distribution of trapped fluids and the total volume of trapped fluid. Inaccurate conclusions about fluid retention properties in porous media can result from improper accounting for or elimination of CEE. A mirroring technique addresses CEE and ensures accurate trapping curve measurements.

Mirroring is used to account for both the entry and exit boundaries. In this case, the portion of the sample near the entry boundary is mirrored or duplicated as if it continues beyond the boundary. This creates a virtual representation of the sample extending in the fluid flow direction. Similarly, a mirroring operation can be applied to the outlet boundary. This involves replicating the portion of the sample near the outlet as if it continues beyond the boundary in the flow direction. By doing this, the simulation effectively considers fluid flow at the digital sample's entry and exit boundaries.

Mirroring in the flow direction offers several advantages. It allows researchers to model a smaller portion of the sample while capturing the influence of both entry and exit boundaries on fluid flow. This significantly reduces the computational resources required for simulations. Additionally, it helps emulate the sample's behavior more realistically, as it considers the entire flow path, especially when capillary end effects or other boundary effects are essential (Hadley and Handy).

2.6 Land and Spiteri Model

Studying the pore-scale description of CO_2 trapping leads to the critical notion of the initial residual (IR) curve. Researchers first examine CO_2 pore-level trapping, considering how CO_2 interacts with the pore structure of the rock. This pore-to-pore investigation sheds light on the basic mechanisms controlling CO_2 entrapment in the underground reservoir.

The process of "upscaling" is the next step to apply this information to bigger scales, such as the centimeter scale of core samples. Averaging the effects seen at the pore level to the larger scale of the core sample is known as upscaling. Historically, this upscaling was carried out to explain the gas trapping characteristics during gas production from the reservoir (Carlon S. Land 1968). Equation 1 shows the IR model put forth by (Carlon S. Land 1968). The irreducible

water saturation is used to equalize the initial and residual CO_2 saturations, and the C coefficient varies depending on the sample

$$S^*_{CO2,r} = \frac{S^*_{CO2,i}}{1 + C * S^*_{CO2,i}}$$

Equation 1

$S^*_{CO2,r}$ and $S^*_{CO2,I}$ represent the residual and initial CO_2 saturation.

The coefficient "C" captures the typical behavior of each rock sample. Equation 1 shows that the trapped saturation and coefficient "C" have a reciprocal connection. Understanding the dynamics of CO_2 trapping in rock formations and optimizing carbon capture and storage techniques depend on this empirical model and its conclusions.

However, the goal of upscaling has changed in the context of CCS initiatives. The ability of the core to trap CO_2 for CCS applications is now the focus. Researchers have attempted to build empirical relationships to determine the amount of initial and residual non-wetting phase saturations (Krevor et al. 2015).

Carlon S. Land's suggestion has been a foundation for additional empirical research in this area. His findings have laid the groundwork for understanding the relationship between the CO_2-trapping behavior and the non-wetting phase's initial and residual saturations in core samples, shown in Figure 7: Land's original trapping curve fits. (Carlon S. Land 1968). Scientists can more accurately determine the potential for CO_2 storage in geological formations and improve carbon capture and storage technologies by examining the IR curve and related empirical linkages. Figure 7 shows Land's original trapping curve fits. They were made using experimental data from several authors that had been published. Note that the plot axes' limitations differ for each case. Axes also display normalized initial and residual saturations, which may exceed 1 for samples that do not initially contain any water

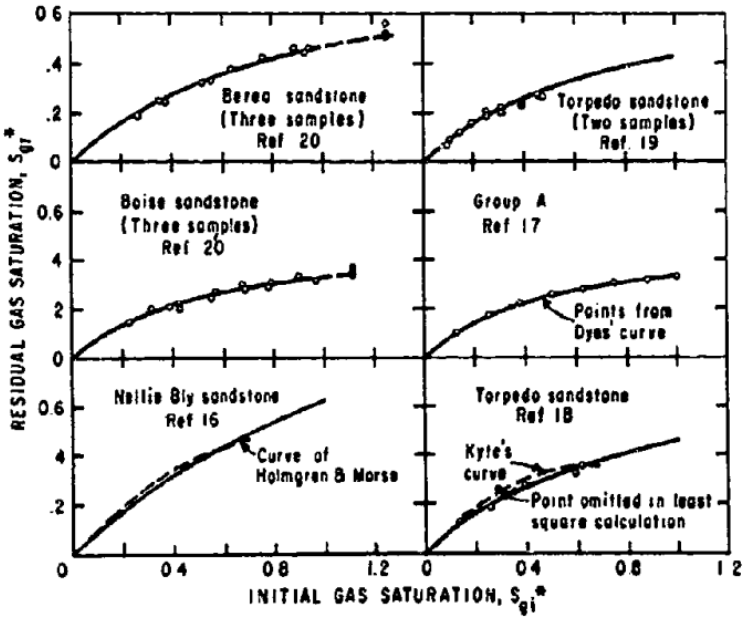

Figure 7: Land's original trapping curve fits. (Carlon S. Land 1968)

Land created an empirical model that connects the initial NWP saturation and the residual NWP saturation for a particular rock. Data from numerous experimental tests found that each rock sample's curves had a unique, recognizable shape, as shown in Figure 7: Land's original trapping curve fits. (Carlon S. Land 1968). By fitting the model to the data, he discovered a distinct relationship between the initial and trapped non-wetting saturation.

Land ran experiments using a variety of initial/residual turning saturation pairings to examine the hysteretic behavior of the system. He started an imbibition flood at various saturation levels, which persisted each time until the remaining NWP saturation was reached. Hysteretic models and scanning curves, a concept first put forth by (Killough 1976), were produced due to this strategy. They focused on hysteretic behavior since capillary trapping depends on it. The study demonstrates that the ratio of residual saturation falls as the initial saturation rises. Due to increased incursion into progressively smaller pores, this suggests that lower amounts of NWP are effectively trapped (Krevor et al. 2015). The research also implies that, after imbibition, these smaller pores are more likely to be the first to be re-saturated with the wetting phase, especially in water-wet rocks.

Figure 9 shows a scanning curve on the left-hand side. The Starting point of each imbibition step is used to create another point, the trapping curve. A slope of one represents a no-flow scenario and therefore 100% trapping.

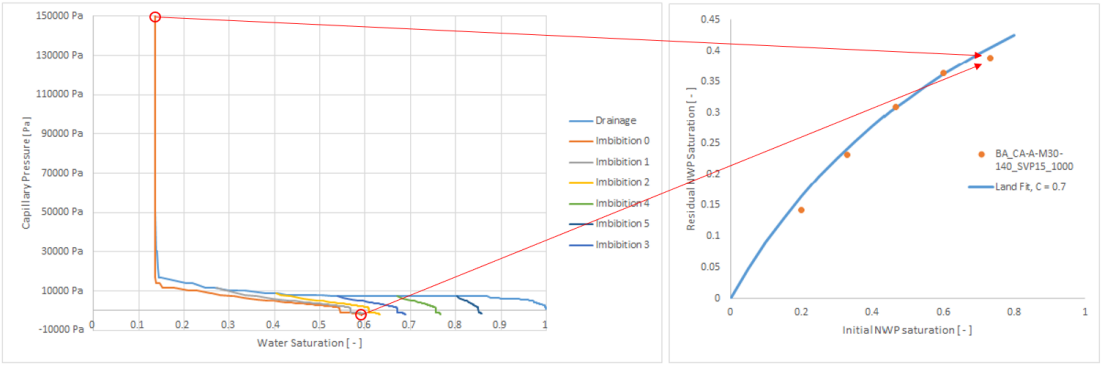

Figure 8: Simulation of a scanning curve (left) with the corresponding Land model fit (right). Red marks indicate initial-residual saturation pairs.

Although the Land model is a fundamental idea and is frequently employed, Spiteri and her team point out that it has limits when utilized with intermediate and oil-wet rocks (Elizabeth J. Spiteri et al. 2008). The model does not account for the crossing of relative permeability scanning curves in intermediate/oil-wet media and fails to represent the genuine nonmonotonic behavior of trapping curves with increasing NWP saturation.

But when combined with other hysteretic models put forth by different authors, such as (Killough 1976), (Larsen and Skauge 1998), and (Hui and Blunt 2000), the Land model is highly accurate and simple to use in water-wet substrates. As a result, the Land model is still a valuable and effective qualitative baseline for evaluating trapping skills.

The bottom and top limits of the Land-parameter "C" based on the degree of heterogeneity were established by Krevor and his team using various rock samples from several studies (Krevor et al. 2015) and are shown in Figure 9. The range of "C" was less when experimental results were only plotted using Berea sandstone, falling between 0.7 and 2. Figure 9 illustrates the range of "C" when carbonate experiment findings were considered, which varied from 0.2 to 5. This significant difference in "C" values between these rocks can be attributed to well-known carbonate heterogeneity, which includes zones with significant fractures versus extremely low-permeability matrix.

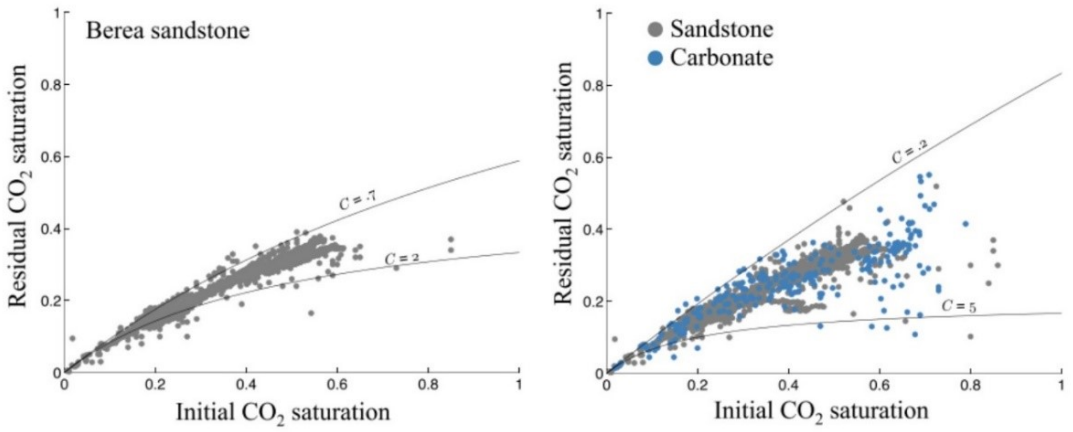

Figure 9: The results of the brine-scCO₂ studies in sandstone are shown in the left plot. The sandstone and carbonate tests are shown on the plot to the right. Solid lines depict the fit of the data-inclusive trapping curves from the Land model. (Krevor et al. 2015)

The study concludes that there may be substantial differences in capillary CO_2 trapping in carbonate reservoirs between various regions of the same reservoir. This conclusion emphasizes the importance of considering rock wettability and heterogeneity when researching CO_2 trapping in geological formations. To better understand these variances and their significance for carbon capture and storage technologies, more investigation and analysis of the database will be conducted in upcoming chapters.

The research project will primarily use experimental and numerical data from numerous studies to test the sensitivity of the outcomes produced by Math2Market's Geodict. Geodict is used to create primary drainage-imbibition hysteresis on digital rock samples. To automate simulations, geodict scripts were written.

Rock-fluid characteristics were purposefully changed during the simulations to simulate various unpredictable outcomes while still being consistent with published experimental data. The Young-Laplace capillary-pressure equation algorithm is used by Geodict's pore morphology method to ascertain the saturation distribution inside the porous media.

Overall, the work seeks to obtain essential insights into the capillary trapping behavior of CO_2 in various rock samples and provide pertinent findings for carbon capture and storage applications by combining experimental data and numerical simulations using Geodict.

2.7 Historical Data

The Geodict software can change parameters for capillary pressure simulations, including contact angle(s) and Interfacial Tension (IFT). The suitable parameter values were chosen based on the experimental findings of different writers. It should be emphasized that in a real-world context, other variables like salinity, pressure, and temperature impact these values. Geodict's performance is unaffected by these aspects because it does not include thermodynamic processes. However, the influence is negligible and can be overlooked for simulations. Additionally, this thesis compares the simulated outcomes by screening databases of Land-model coefficients. For further reading, sources for the experimental findings and coefficients are given.

Contact Angle

The contact angles of various minerals (quartz, calcite, and muscovite) were measured experimentally, and visualized in Figure 10, Figure 11, and Figure 12 by Farokhpoor et al. under various brine salinity, starting pressure, and temperature conditions. Their research shows that the contact angle varies greatly depending on each parameter. Pressure impacts contact angles up to the critical point, after which it has little effect on contact angles overall across all mineral kinds. Mineral wettability is somewhat reduced when salinity increases. Depending on the mineral type, the effect of temperature ranges from negligible to significant.

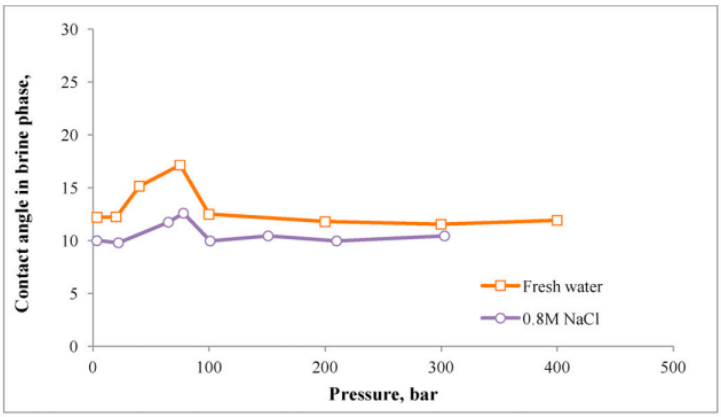

Figure 10: CO_2–brine contact angle on calcite surface (Farokhpoor et al. 2013)

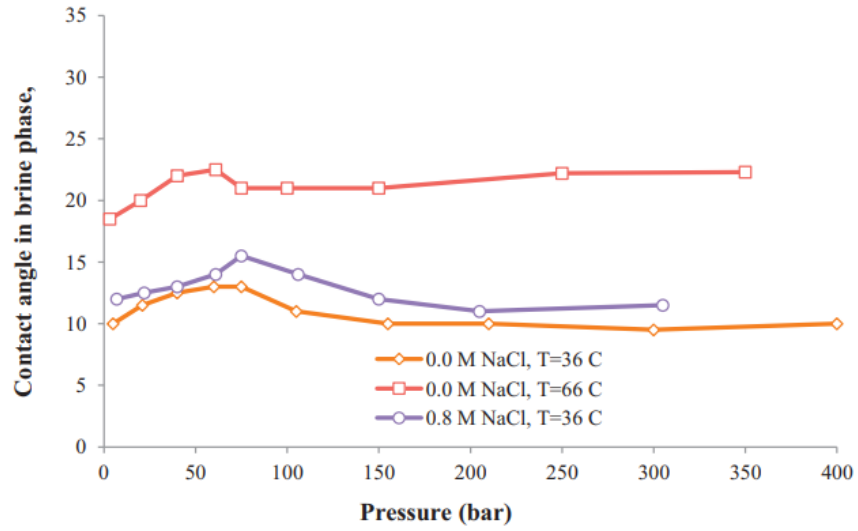

Figure 11: Pressure against CO_2-brine contact angle on the quartz surface. (Farokhpoor et al. 2013)

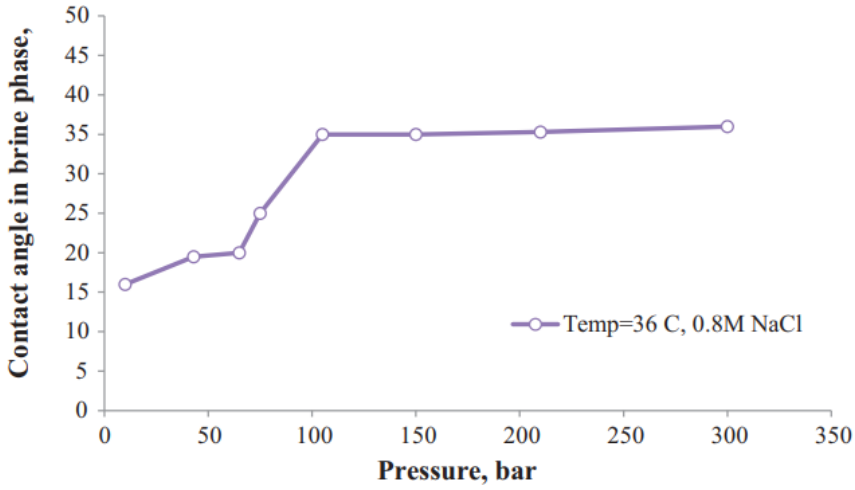

Figure 12: Pressure against CO_2-brine contact angle on muscovite mica surface. (Farokhpoor et al. 2013)

Calcite, quartz, and muscovite mica are the three surfaces on which CO_2-brine has the greatest contact angle. All three figures correlate the contact angle and pressure. Furthermore, the findings of (Saraji et al. 2014) quartz investigation align with those of (Farokhpoor et al. 2013). Both investigations in Figure 13 and Figure 14 show similar contact angles from 10° to 40°. (Krevor et al. 2015) investigated the Mercury Intrusion Capillary Pressure (MICP) curve fitting to the CO_2-brine system using an IFT of 34.5 mN/m and a sensitivity range of contact angle/s of 50°+-10° to give an alternate strategy based on data fitting. They established a reliable fit by comparing their experimental findings to the fitted MICP curves, proving that the values discovered during the fitting procedure are accurate. As a result, this study and the earlier

described research can be used to determine the simulation values that are frequently encountered.

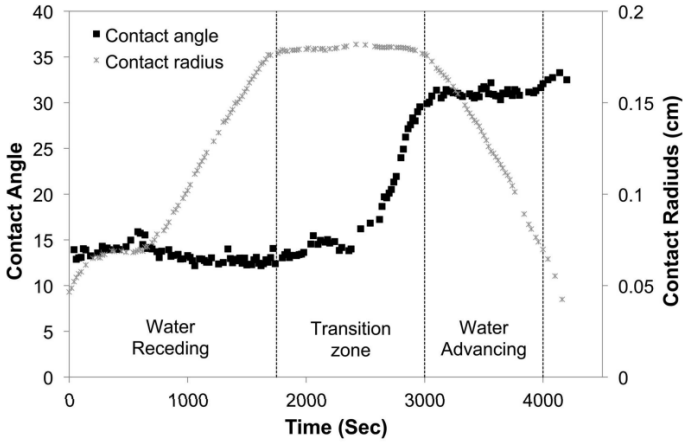

Figure 13: CO_2 bubble on quartz in water at 1700 psi and 60°C produces a receding and advancing contact angle. (Saraji et al. 2013)

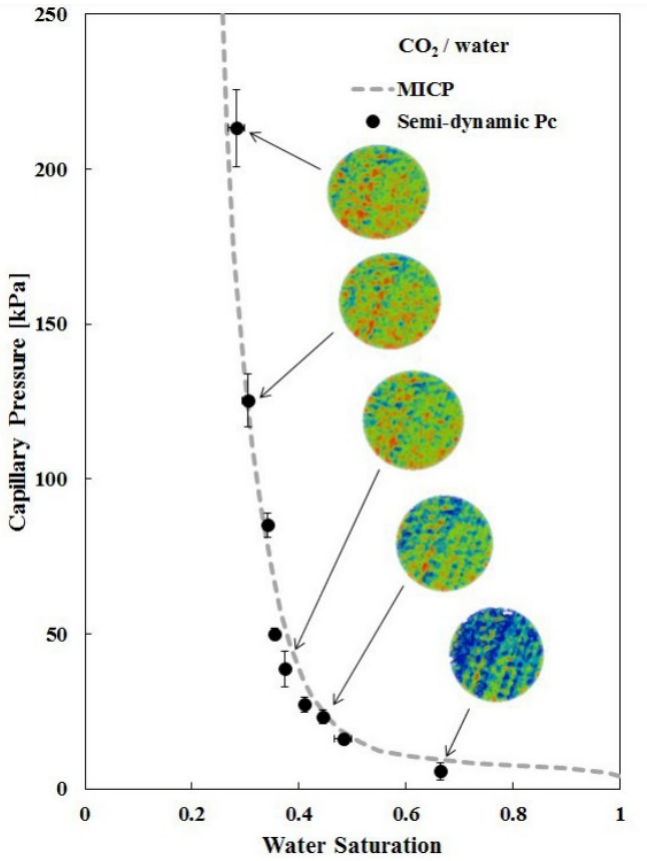

Figure 14: An illustration of a CO_2-water capillary pressure test from (Al-Menhali and Krevor 2014) is shown in black dots

Interfacial Tension

IFT is frequently an essential parameter to research in EOR (Arnold 2018). IFT, however, only functions as a scaling factor in Geodict. This means that the Young-Laplace equation employed in SatuDict only considers the influence of the geometrical pressure, and the IFT only affects the pressure that results. For instance, altering the IFT won't affect the capillary pressure curve or make it possible to access smaller holes. IFT will, therefore, be treated as a constant variable with a value of 35 mN/m, comparable to the values frequently seen in tests for the $scCO_2$-brine system. Examples of these values from the literature are shown in Figure 15 and Figure 16 from Saraji et al. and Al-Menhali and Krevor, respectively.

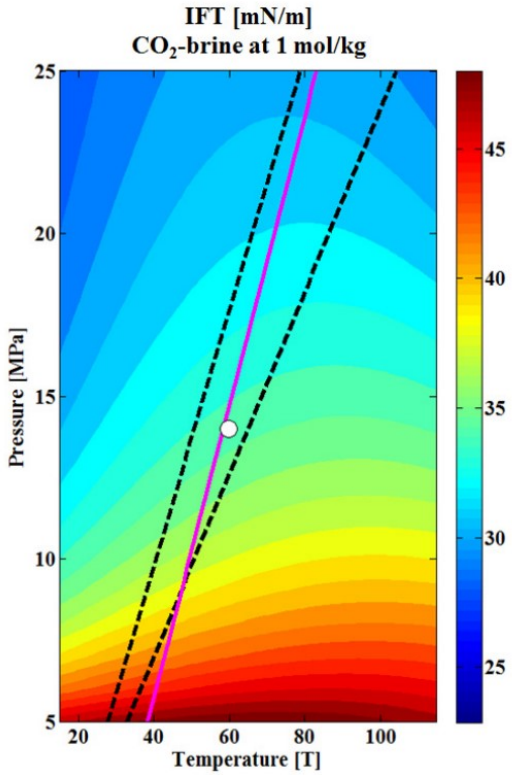

Figure 15: The white circle indicates the experimental situation. Contours depict CO_2-brine's interfacial tension at 1 mol/kg. Assuming surface temperatures of 15°C for the US and 27°C for Qatar, respectively, and a hydrostatic pressure gradient for both, the solid Magenta and dotted Black lines show the range of geothermal and hydrostatic gradients in Qatar and the US (Al-Menhali and Krevor 2014)

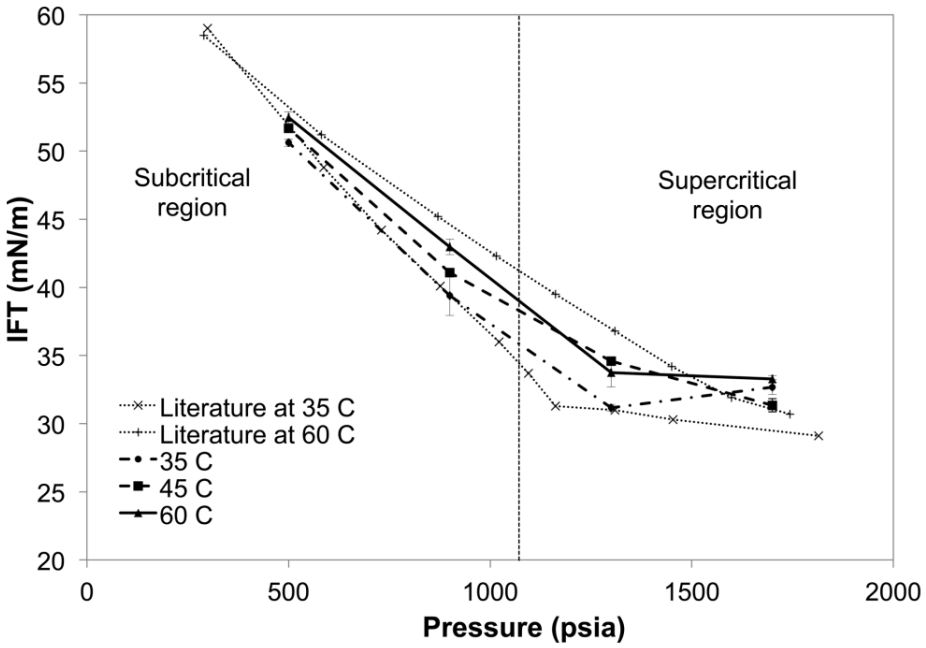

Figure 16: IFT literature values. (Saraji et al. 2014)

Land-model constants

The trapped phase and its initial saturation can be related empirically using the Land model, as was previously stated. If the wetting circumstances stay the same, this relationship should hold for a particular rock sample. Significant trends for diverse rock samples might be found by examining numerous datasets from various authors. It has been noted that the constant is smaller for samples wet with water than those wet with intermediate or oil. The outcomes from this investigation will be analyzed using the literature results shown above in Figure 7: Land's original trapping curve fits. (Carlon S. Land 1968) as a guide.

Depending on the type of rock and how wet it is, the constant value in the Land model describes the connection between the trapped non-wetting phase and early saturation changes. The literature provides a wide range of constant values, from Land-values greater 5 for oil-wet carbonate rocks to 0.2 for very water-wet sandstone. Since the rocks employed in this study are sandstone, the significant variability is primarily attributable to carbonates. Therefore, for sandstones, with a range of Land-constant values between 0.7 and 2, comparing this work with the literature is more appropriate. However, it may be inferred that the Land model constant values range should be between 0 and 6, even with high rock property variability. The projected range of constant values is smaller based on the inherent characteristics of the rocks employed in this investigation, indicating more uniform characteristics. This will be covered in the following chapters, along with a presentation of the digital rocks utilized in this study and the procedure.

(Krevor et al. 2015) and their team developed a database that specifies the limits of Land-parameter C based on the degree of heterogeneity after several trials on various rock samples. The range is considerably smaller, ranging from 0.7 to 2, when concentrating only on experimental outcomes using Berea sandstone. The range of the Land-constant varies from 0.2 to 5, though, when carbonate experiment data are considered. Due to well-known carbonate heterogeneity, such as wettability fluctuations, large cracks, or a deficient permeability matrix, this significant variance exists. Thus, it may be inferred that capillary CO_2 trapping in carbonate reservoirs may differ significantly between various regions of the same reservoir.

Chapter 3

Technical Chapters

The effectiveness of the Morphological Method depends on several factors, including the contact angle, contact angle distribution method, domain size, order of experimental procedure, and stochastic versus deterministic approach. These factors can significantly impact the outcome of morphological method experiments, and it is essential to understand their effects to ensure accurate results.

This chapter will discuss these different approaches to the outcome of morphological method experiments. We will explore the effects of different contact angles, contact angle distribution methods, and domain sizes on the results obtained from morphological analysis. Additionally, we will examine the importance of the order of experimental procedures and the difference between stochastic and deterministic approaches in morphological analysis.

Through our investigation, we hope to provide insights into the various factors that can influence the outcome of morphological method experiments. By understanding these factors, researchers can optimize their experimental protocols to obtain the most accurate and reliable results.

3.1 Methodology

The computational environment's foundational principles are briefly explained at the beginning of the workflow description to ensure readers are familiar with the program and how calculations are carried out.

This thesis uses Geodict, a multi-scale 3D image processing program, to run simulations. It is helpful for modeling processes in porous media. It applies to prior publications by Arnold et al., Alexandru-Mihai Badescu, Mario Dragovits, and Lobel Zvonimir Danicic that studied porous media scientifically.

There are several modules in Geodict, but the SatuDict module is used to obtain the desired trapping curves by deriving capillary pressure curves. The improved morphological method described in (Hilpert and Miller 2001), covered in the Literature Review section, is the foundation of SatuDict. This method calculates the fluid distribution using the Young-Laplace equation in terms of the radius remains constant. The distribution of pores in the used structure is ultimately what determines this.

The forced imbibition tool is the primary tool used to create trapping curves in this thesis. The instrument's effectiveness and physical representation of saturation-dependent processes were confirmed by research (Lobel Zvonimir Danicic 2022). The created workflow, as shown in Figure 17 is composed of the subsequent deliberate steps:

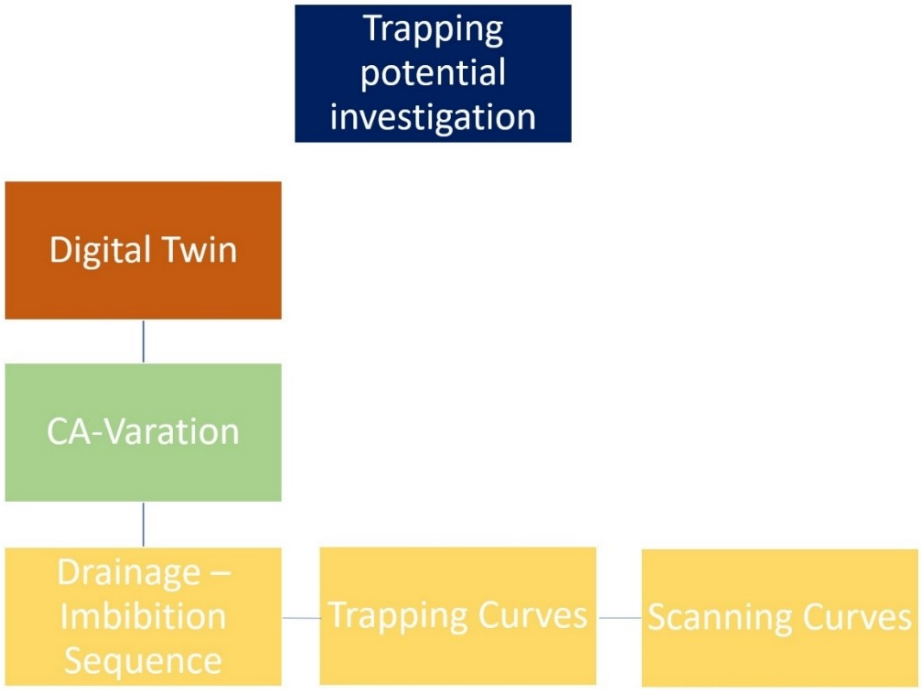

Figure 17: General workflow in DRP before the implementation of the effect of forced Imbibition

To account for the force imbibition part and its significant effects within the hysteresis, the workflow had to be adapted and is shown in Figure 18. The implementation of the Solid Volume Percentage (SVP) represents the impact that forced imbibition has on the whole process.

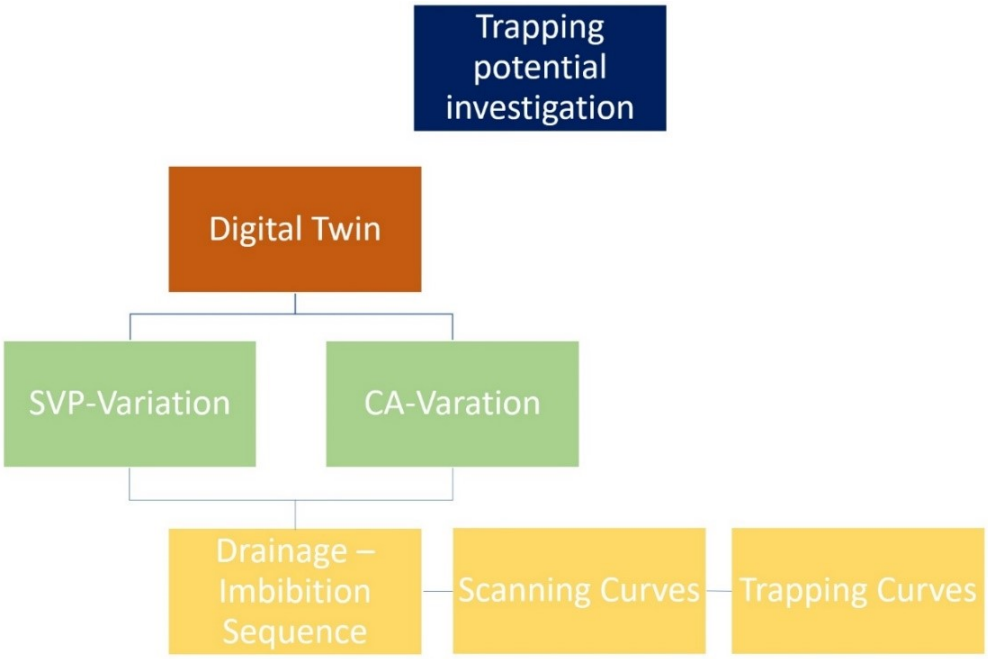

Figure 18: Workflow in DRP with the implementation of the effect of forced Imbibition

3.1.1 Drainage and Spontaneous Imbibition

In a porous medium, primary drainage is the WP displacement by the NWP. This process is defined by a series of stages that imitate the invasion caused by an applied differential pressure and flow constraints at the pore mouths. The idea is demonstrated using a simple 2D porous structure with round grains in gray and the WP-filled pore region in blue.

The three actions stand for a single displacement event. In the first phase, grains are dilated to locate and seal the smallest pore mouths. As shown in Figure 19, the invaded NWP is connected to this reservoir and changed to dark green. The NWP reservoir is defined on the left side. In this step, the pore space containing NWP is identified.

The Young-Laplace equation:

$$p_c = \frac{2 * \sigma * \cos\theta}{r}$$

Equation 2

The capillary pressure p_c is impacted bythe interfacial tension σ, the contact angle θ,, and the pore throat radius r.

The basic drainage algorithm can be changed to mimic imbibition processes by making a few modifications. In stages 2 and 3, the roles of the NWP and WP are reversed to mimic imbibition. In addition, the NWP and WP are exchanged in Dilation step 2 instead of the Drainage

operation. The enhanced method for imbibition is shown in Figure 19 and described by Arnold et al.

These adjustments allow the algorithm to model the imbibition process, in which the WP invades the pore space previously saturated with the NWP. The NWP is dispersed during imbibition, and any NWP separated from the reservoir is regarded as residual and does not further the fluid displacement. (Arnold et al. 2023).

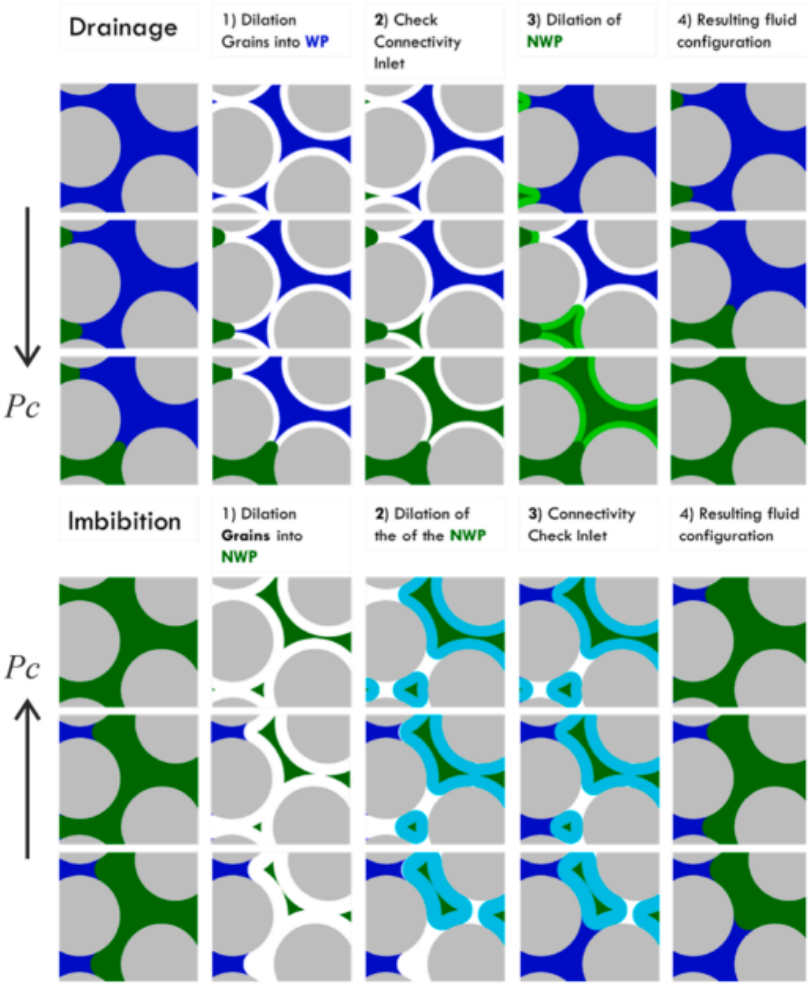

Figure 19: The drainage (top) and imbibition (bottom) algorithms are shown in a simplified 2D diagram. In both instances, the front encroaches from the photos' left side. The NWP is shown in green, whereas the WP is shown in blue. When there is drainage, the capillary pressure, or p_C, rises; when there is imbibition, the pressure falls. (Arnold et al. 2023)

Forced Imbibition

The influence of forced imbibition on the imbibition process is realized by including a second material with a different wetting phase.

The NWP is dilated by the same voxel radius as the grains in the previous stage in the following phase. The invading NWP during drainage first invades the larger pore throats, which prevents it from passing through the first pore throat.

Figure 20 shows that the invasion phase can overcome the same pore throat using Multiple Contact Angles (MCA)NWP in the same situation since the dilation is scaled by cos(θ). The result is that the same applied pressure leads to many invasion paths. Additionally, the NWP (green) has a different contact angle for each substance in this process.

The invading NWP must be connected to the intake phase, the NWP reservoir, throughout the drainage process, and the WP must be connected to the outflow, which is the WP reservoir. Understanding the behavior of fluid displacement, capillary forces, and the impact of contact angles on fluid invasion and distribution inside the porous media is made possible by this procedure.

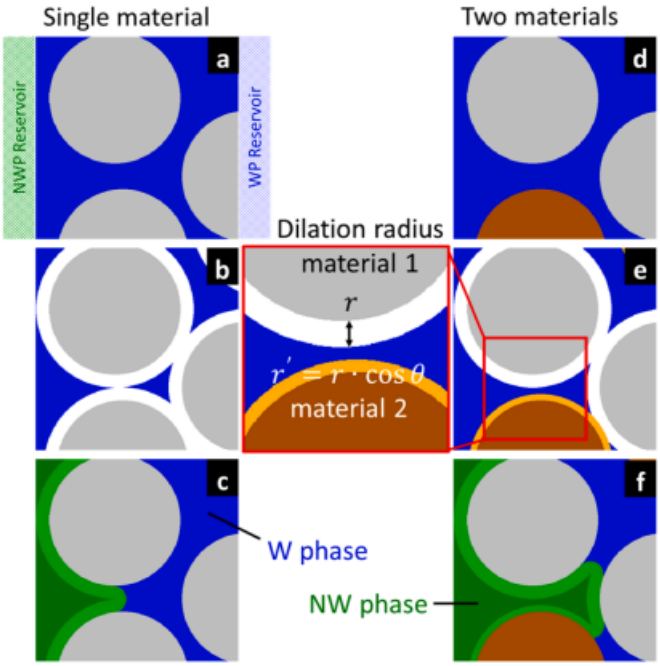

Figure 20: Simple representation of a drainage invasion step for two materials with varying contact angles (d-f) and one with a single contact angle (a-c). The nonwetting phase is colored green, the wetting phase is colored blue, and the solid mineral phases are colored gray and brown. Lighter hues are used to denote dilated volumes. (Arnold et al. 2023)

The drainage process is carried out initially in the simulation of imbibition processes utilizing the pore MM. The invasion of the NWP into the porous media is represented by the drainage process, identified by wholly positive capillary pressure. However, two distinct characteristics emerge during the imbibition process: an early saturation range with positive capillary pressure

and a late saturation range with negative capillary pressure. Negative capillary pressure denotes a forced action analogous to drainage.

Spontaneous Imbibition and Forced imbibition (FI) procedures record the entire saturation range in the pore MM. When the NWP is snapped off from the outlet, the SI process ends, trapping the material and preventing further displacement by drainage or imbibition. A non-wetting substance is added to scale the shift from SI to FI by obstructing the spontaneous process's access to some areas of the pore space. Two different approaches can be used to introduce the non-wetting material. Those are the stochastic and the deterministic approach which are explained in more detail, in the following chapters.

Stochastic Approach

The parameters for the stochastic field are defined in the stochastic approach, such as the volumetric percentage and region size. An isotropic Gaussian random field is then employed to implement the material distribution utilizing this stochastic field as a foundation. Nonwetting materials are realistically applied utilizing two distinct region sizes, as indicated in Figure 21. Nonwetting materials are realistically applied utilizing two distinct region sizes. An identical random seed was used in both cases. However, one scenario's region size was smaller, and the other was bigger than the typical visible grain size. The supplied material will inevitably establish interconnections across the structure depending on the size of the selected region and the SVP. Notably, with a few minor variations, the change in material volume percentage is identical to the difference in surface area between porous and solid materials. (Arnold et al. 2023)

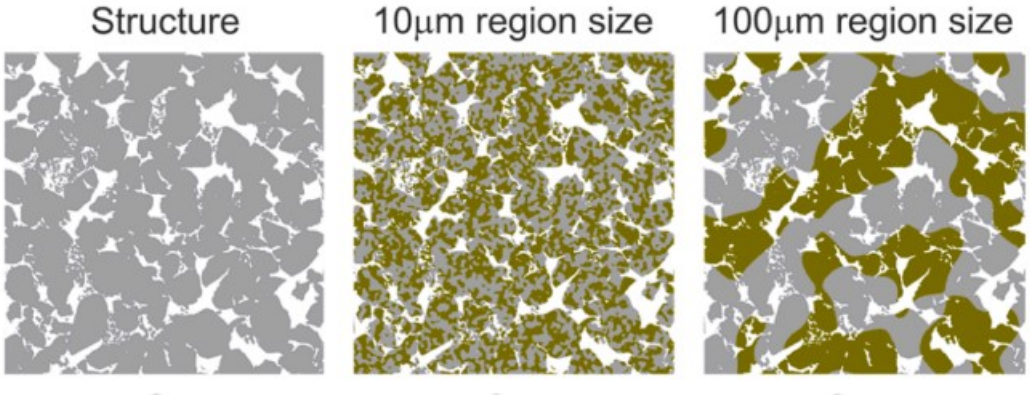

Figure 21: A wettability-modified and unmodified example of the Berea rock structure. A scan's stochastic field is used to add a second material. With various region sizes of 10 m (middle) and 100 m (right) and a SVP of 50% in both cases, the yellow material. (Arnold et al. 2023)

Before the start of drainage, the nonwetting material is delivered based on a stochastic field to ensure contact between the nonwetting material and the NWP by the end of the drainage

process. Alternatively, nonwetting material can be added after draining, but only in the pores that the NWP has already occupied. The biggest pores are given priority in this introduction.

Deterministic Approach

The natural phenomena of wettability modification over time, wherein mineral surfaces interacting with the NWP can change their initial wetting characteristics, is the basis for the deterministic approach. This methodology uses an algorithm to examine the distribution of pore sizes after a drainage operation. After that, nonwetting material is first introduced into the biggest pores, specifically where the mineral and NWP interact.

Only NWP-filled pores receive non-wetting material after drainage, with the most significant holes receiving priority. This strategy replicates the wettability alteration that occurs naturally as minerals interact with the NWP over time, changing their original wetting state. (Arnold et al. 2023).

3.2 Workflow

3.2.1 Adaption of the Methodology

Surface characteristics like wettability and contact angle distribution are the driving phenomena in spontaneous imbibition. It is essential to consider how well the MM captures these physical processes. When a single contact angle dominates, the invading fluid's course through the porous domain is consistently determined, regardless of the contact angle. Therefore, changes in the contact angle do impact the order of invasion, fluid distribution, or subsequent relative permeability curves.

The integration of various contact angles was a topic Schulz et al. (2015) addressed in their work. They altered the invasion process by altering dilation radii using the cosine of the contact angle (a). However, because dilation approaches zero at these limits, they limited the system to contact angles below or above 90 degrees. Negligible numerical errors were seen at contact angles less than 60 degrees or greater than 120 degrees. Diverse displacement pathways become possible with the inclusion of different contact angles.

The moment when wettability distribution is introduced significantly impacts how fluid phases behave. The wettability distribution changes due to the non-wetting phase being forced out of the bigger pores and confined in the smaller ones. (Lobel Zvonimir Danicic 2022) investigated distributions solely before primary drainage and missed out on impacts of fluid distribution and impact of order of invasion. Therefore, it is essential to consider the distribution following primary drainage to forecast fluid behavior during subsequent imbibition processes. This helps

us to better understand the physical procedures in fluid flow and transport in porous surfaces, allowing us to make predictions about reservoir behavior that are more precise.

Figure 22 shows the workflow of a trapping potential investigation, after adapting it to new procedure. It considers that we do not deal with a change of wettability within the digital twin, and accounts for the impact of forced imbibition. This is done by the SVP, based on a stochastic distribution.

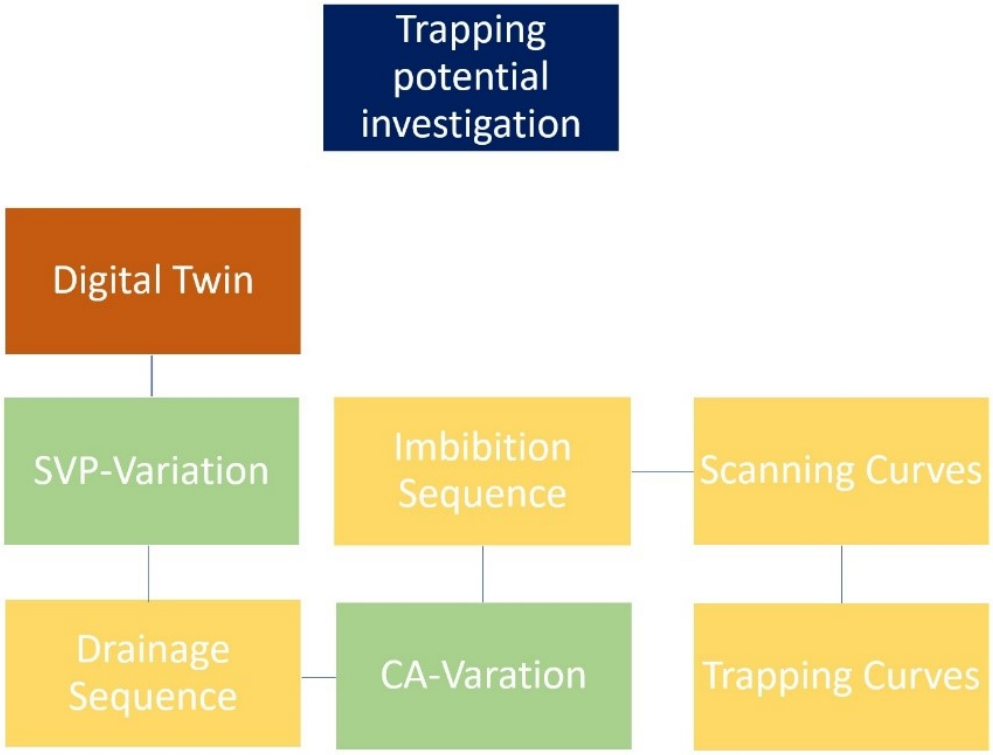

Figure 22: Workflow in DRP with the adapted It workflow to better account for the effect of forced imbibition, but taking into account that no real wetting change in a CO_2–water system is assumed

3.2.2 Land Benchmark

Krevor et al. experiments in Figure 9 are used as a benchmark to define the lower and upper boundaries of the Land-parameter. The primary objective was to identify the representative elementary volume within predefined parameter limits. Specifically, when focusing solely on Berea sandstone in experiments, the values ranged from 0.7 to 2, establishing these values as the acceptable range based on heterogeneity.

3.2.3 Domain Size

The simulations mainly occurred inside a 500^3 voxel domain. The biggest obstacle in running simulations on a 1000^3 domain size is their significantly longer runtime. A 500^3 voxel domain correlates to a millimeter-scale rock formation. There is a potential issue with numerical border

and capillary-end effects in these smaller simulation environments. These factors might result in nonphysical saturations and discrepancies between the simulated data and the Land model.

On the other hand, using a domain size of 500^3 offers a significant benefit by allowing the execution of numerous simulations in a short amount of time. This domain dimension might offer insight into the potential value of devoting more time and resources to certain samples.

Simulations were run on a larger, 1000^3 voxel domain to examine the impact of domain size. The domain size is increased to lessen the influence of CEE and incorporate a more accurate pore size distribution. Additionally mirroring effects were applied to those domains. When even doubling the domain length in flow direction, did not show any significant changes, the REV was established.

3.2.4 Scanning & Trapping Curve

In digital rock physics, scanning curves, often called drainage and imbibition curves or hysteresis, are crucial for examining the behavior of porous media in the petroleum sector. They are acquired by mimicking controlled fluid flow through a digitally recreated rock sample. The amount of fluid that can be removed from a rock sample as the pressure is reduced is measured using drainage curves. Imbibition curves, on the other hand, quantify how much fluid can be added to the rock sample as the pressure rises. We can create a scanning curve by moving the starting point of each imbibition point alongside the drainage curve.

Scanning curves, such as in Figure 23, are generated in digital rock physics through numerical simulations that closely resemble the experimental parameters of drainage and imbibition processes. The critical entry pressure, the residual saturation, and the pore size distribution of the rock sample can all be extracted from the scanning curves. The initial and residual saturations, resulting from the varying starting points, can then be fitted into the land model.

Figure 24 visualizes the impact of forced imbibition (increase of SVP) on a single trapping point. Where the hysteresis shows a faster transition towards negative capillary pressure, we can observe a steady downward trend in the trapping curve.

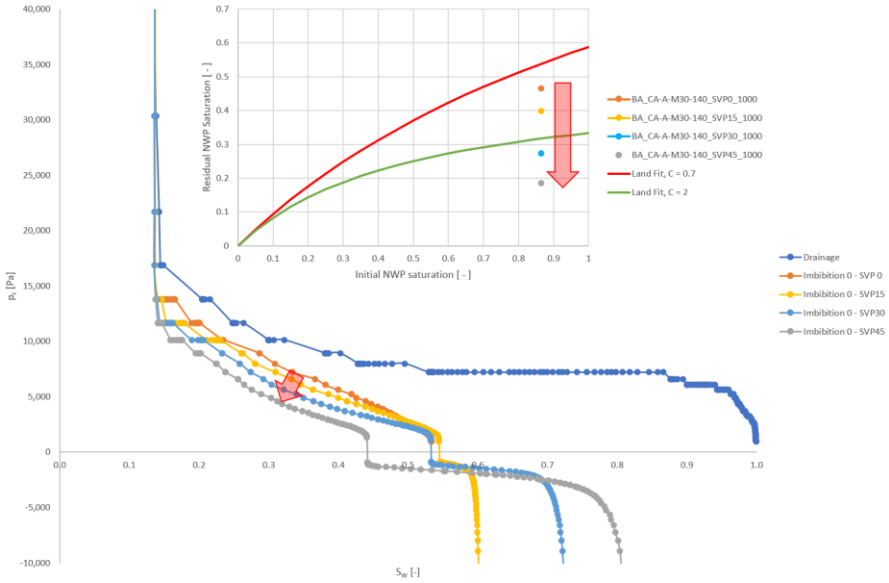

Figure 23: Impact of the increasing impact of forced imbibition (SVP) for the BA_CA-A-M30-140 case and its effect on the trapping curve.

Creating capillary trapping curves from scanning curves involves analyzing simulated data to understand how a porous medium retains one fluid phase when another displaces it. The process involves plotting capillary pressure and saturation. To get started, a graph where the x-axis represents the saturation of one of the fluids usually, the non-wetting phase. The y-axis represent the capillary pressure. Each data point on the graph corresponds to a specific saturation-capillary pressure pair. Next, pinpoint the point on the graph where the saturation change equals zero. This point corresponds to the irreducible saturation of the wetting phase, representing the saturation level below which the non-wetting phase cannot further displace the wetting phase. To calculate the trapped phase saturation, find the difference between the total saturation of the non-wetting phase (1 - irreducible saturation) and the residual saturation. This value represents the fraction of the non-wetting phase retained within the porous medium due to capillary forces. Now, plot the trapped phase saturation on the y-axis against the saturation of the non-wetting phase on the x-axis. This capillary trapping curve reveals how the trapped phase saturation varies with non-wetting phase saturation. A steeper curve may indicate higher capillary trapping efficiency.

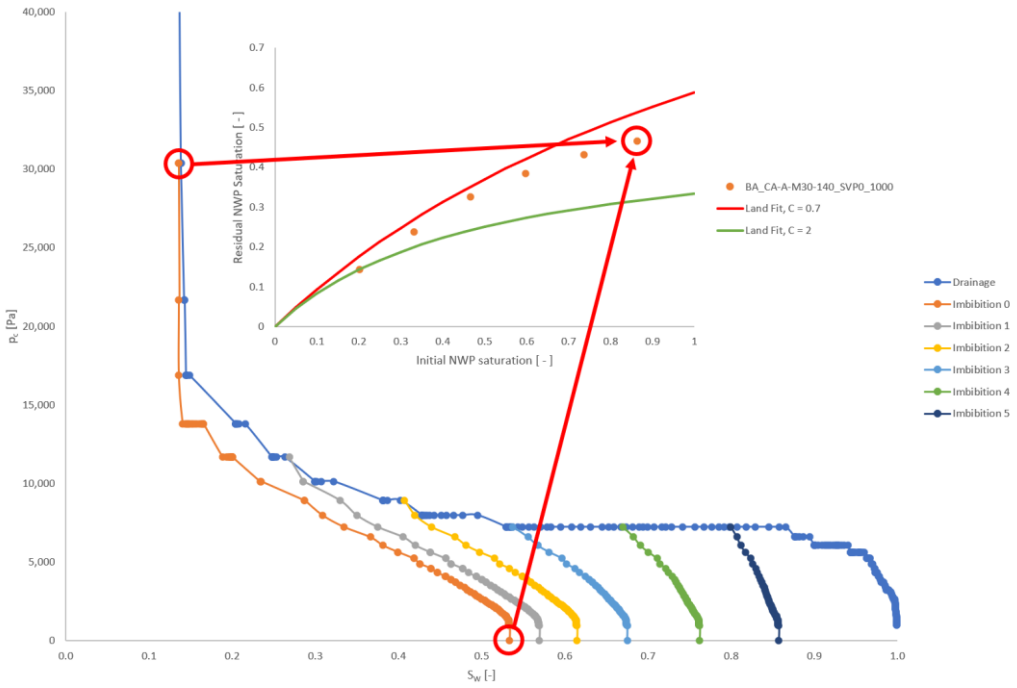

Figure 24: Visualization of the process to create a trapping point from a scanning curve for the BA_CA-A-M30-140_SVP0_1000 case.

3.3 Experimental Nomenclature

The studies were evaluated qualitatively, and alternative experimental setups were compared with changes to several factors. The following is what those acronyms mean:

BA_CA-A-M10-140_SVP45_500

BA: stands for the used rock sample, the Berea sandstone.

CA: is the indicator for the Contact Angle and its methods

A: Contact angle distribution after primary drainage

B: Contact angle distribution before primary drainage

M: Multiple Contact Angle method

S: Schultz Method

10: The first number indicates the contact angle of the wetting material

140: The second number indicates the contact angle for the nonwetting material

SVP45: Is the Solid Volume Percentage (SVP). It impacts the influence of the forced imbibition, and indicates the percentage of rock structure changed to NWP.

AG: Deterministic Approach with varying pore volume that is considered for a change of wetting material

500: the last number refers to the domain size on which the experiments were conducted. 500 stands for a 500x500x500 domain size.

Chapter 4

Results and Discussion

Results will be addressed and presented in this section. We'll start off by looking at scanning curves. They are a crucial component of the capillary trapping curve construction process. The effect of FI on those curves will be presented in more depth.

The methodology will next be tested by reproducing the curves from our starting point. We will introduce an enhanced CA distribution method and go into great depth about how it affects the capillary trapping potential using this workflow. Before we demonstrate the impact of domain size and afterwards the development of mirrored ways to limit CCEs and establish a REV with the developed approach, the impact of the stochastic and deterministic distribution will be demonstrated.

4.1 Scanning Curves

The visualization of this process is shown in Figure 26, Figure 27, Figure 28, and Figure 29, showing that the increase of the SVP from 0% to 45 % in increments leads to the shift of the imbibition curves. This is notably visible when the capillary pressure reaches negative values. The imbibition curves, as shown in Figure 30, also reach negative values earlier, the higher the impact of forced imbibition is accounted for.

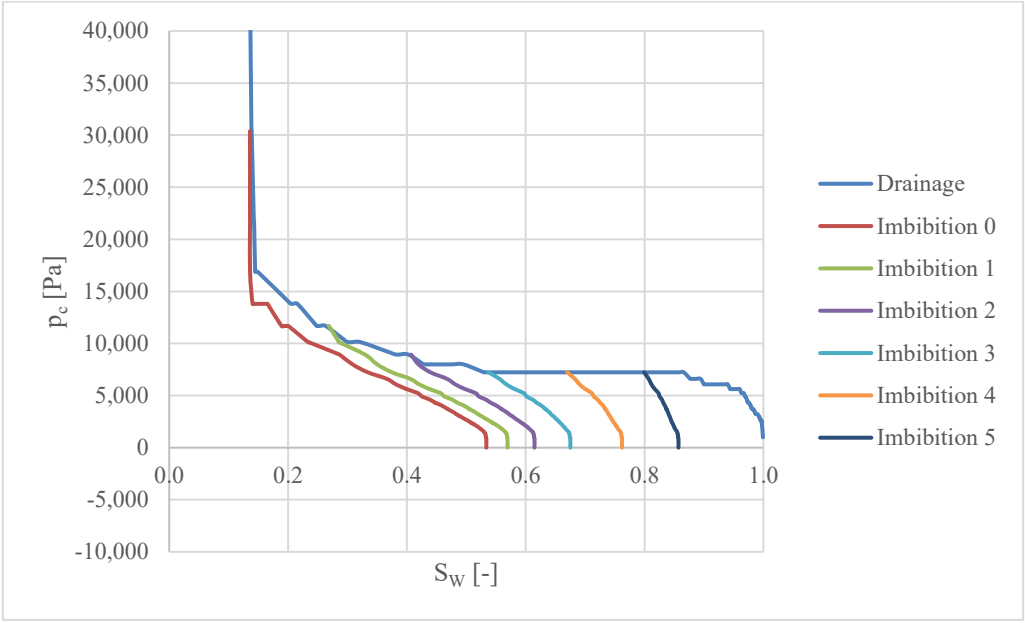

Figure 25: Scanning curve for a simulation case with a 30-140 contact angle and an SVP of 0.

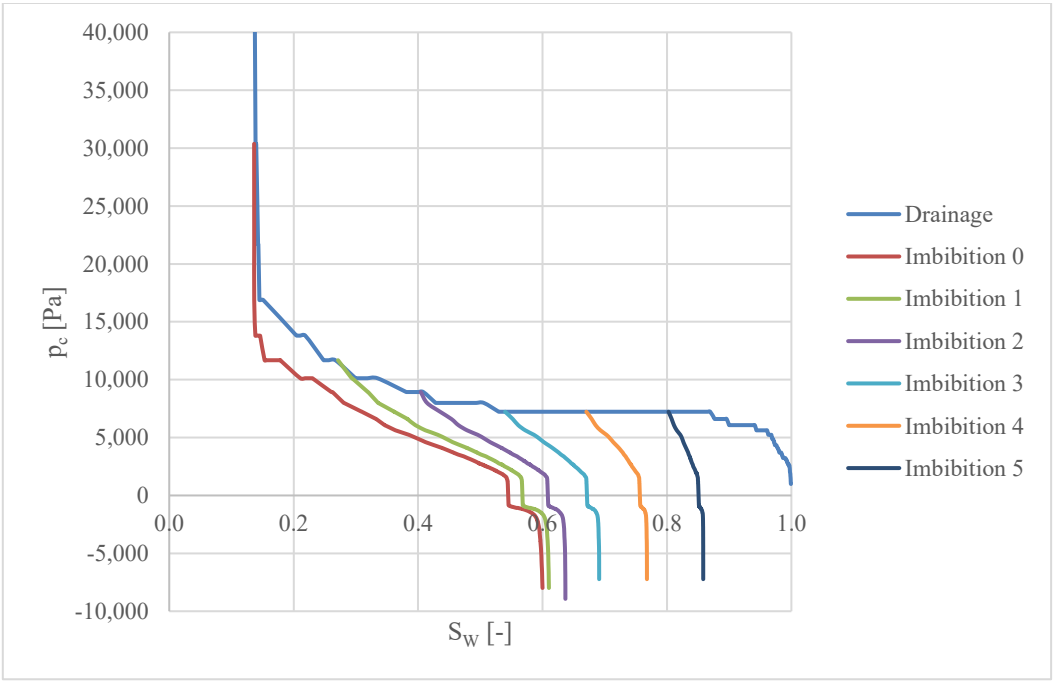

Figure 26: Scanning curve for a simulation case with a 30-140 contact angle and an SVP of 15.

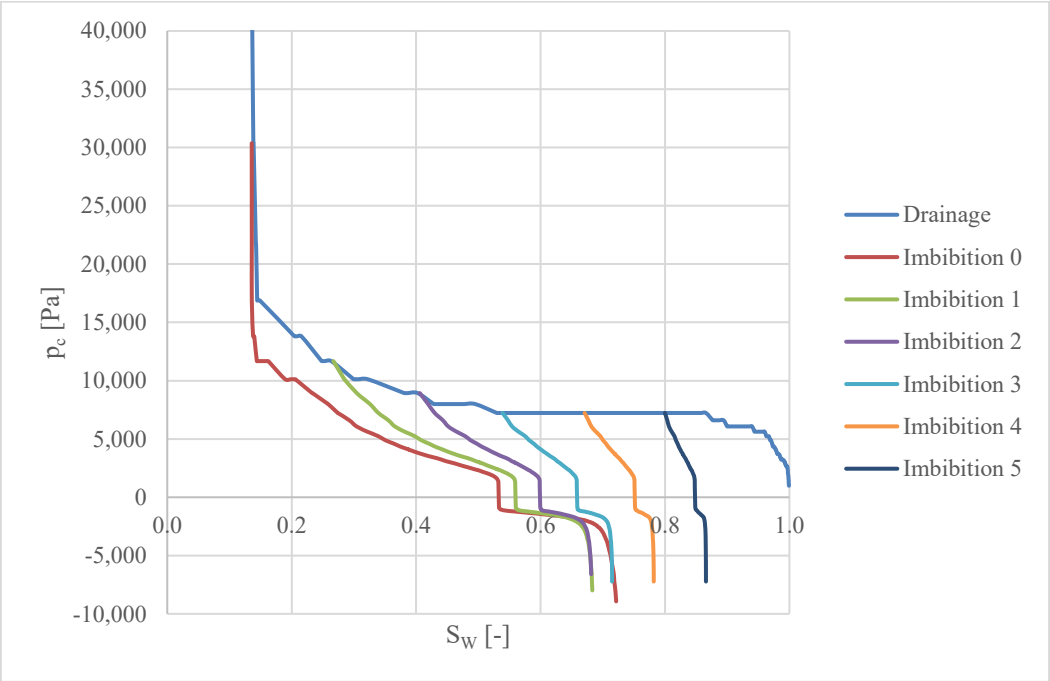

Figure 27: Scanning curve for a simulation case with a 30-140 contact angle and an SVP of 30

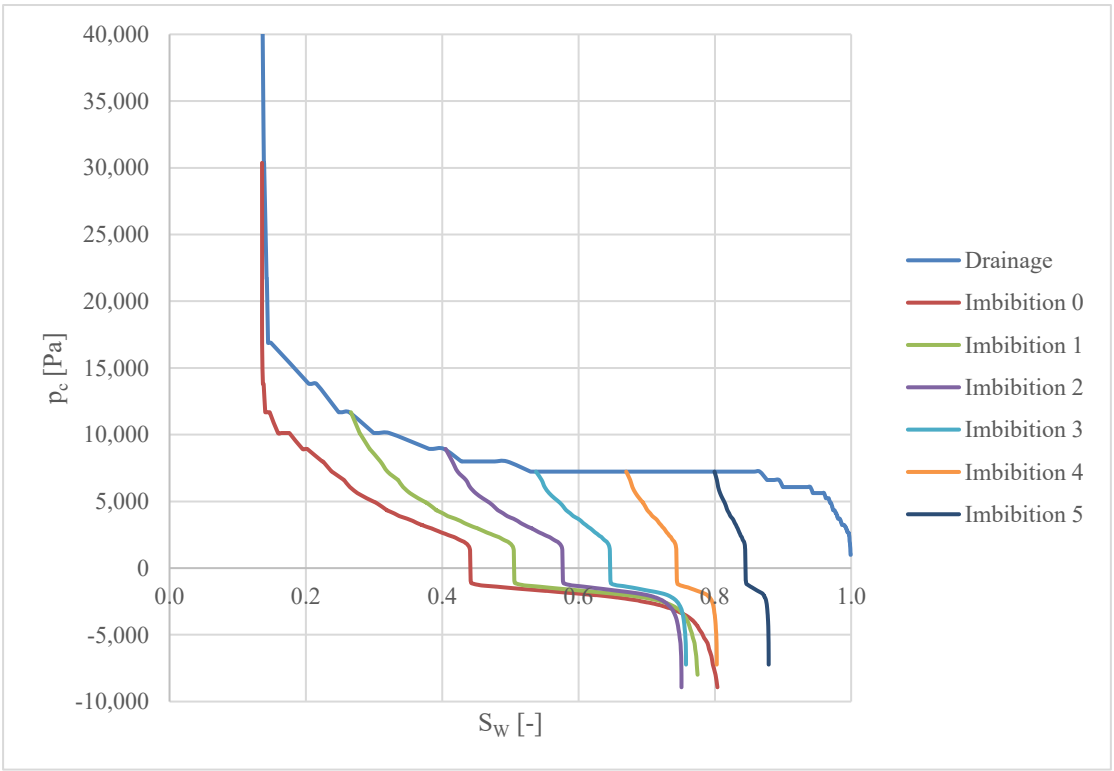

Figure 28: Scanning curve for a simulation case with a 30-140 contact angle and an SVP of 45

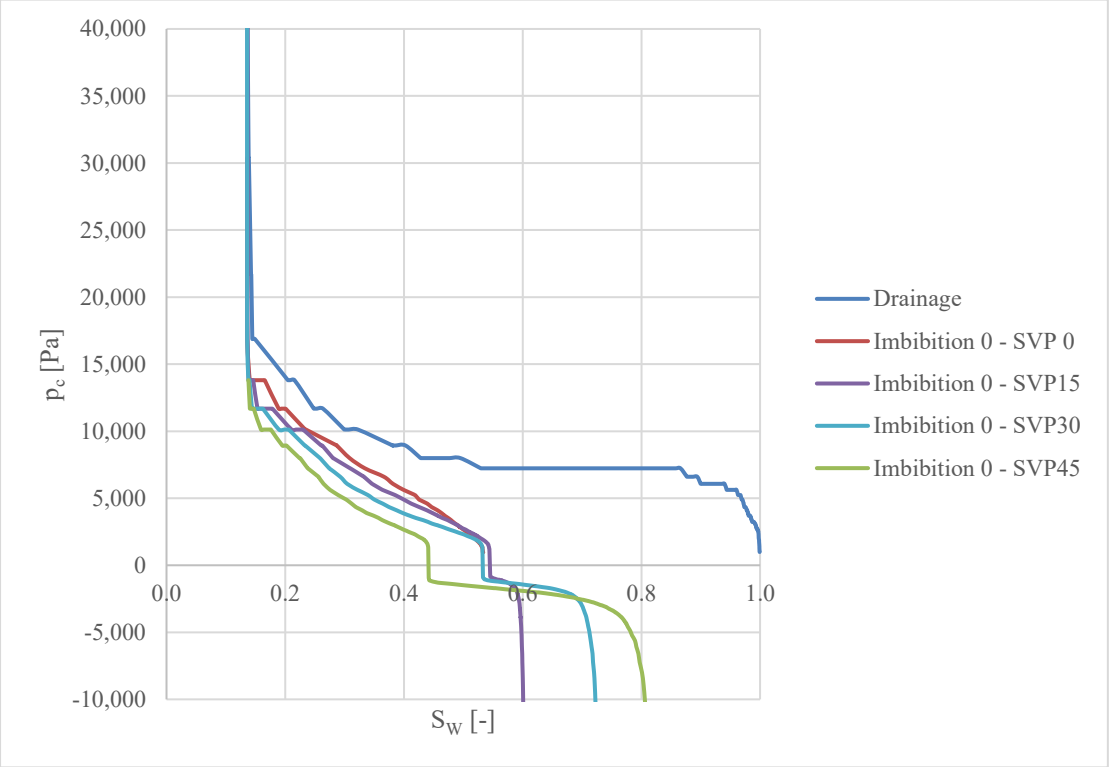

Figure 29: Scanning curve for a simulation case with a 30-140 contact angle and an SVP of 0 to 45 for the first imbibition step of each experiment.

4.2 Trapping Curves with Previous Approaches

Previous simulations by Lobel show that the Land-model parameter successfully captures the upper (C=1.15) and lower (C = 11) boundaries. While the lower limit is noticeably skewed, the top boundary coincides with the indicated range of experimental results. Plots exhibiting parameter-by-parameter relationships will be shown in the following section. Since significant adaptions were done in the Geodict workflow by Math2Market, the first step was to ensure the reliability and reproducibility of prior experiments. Therefore, the most reliable experiments from (Lobel Zvonimir Danicic 2022) were chosen and visualized in Figure 32 and Figure 33. They show a definite influence of SVP. Capillary trapping decreases in direct proportion to an increase in SVP. As SVP values increase, this tendency is accompanied by a decline in the variation of curves among various samples. The range of C values ranges from 2 to 8, even though trapping curves tend to cluster near the lower end. Due to the scale's nonlinear nature in the Land model, this distinction might not be immediately apparent.

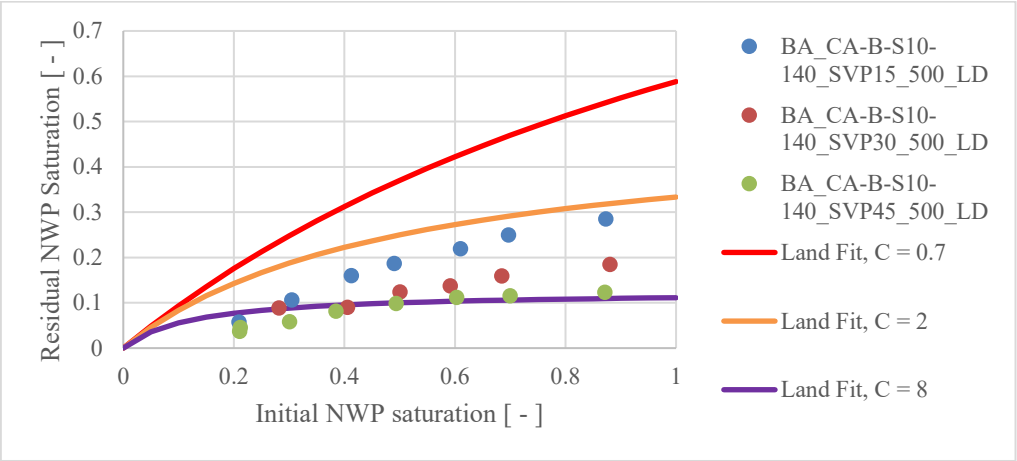

Figure 30: Reproduced trapping curves for 10° and 140° contact angles and an SVP range of 15 - 45%. (Lobel Zvonimir Danicic 2022)

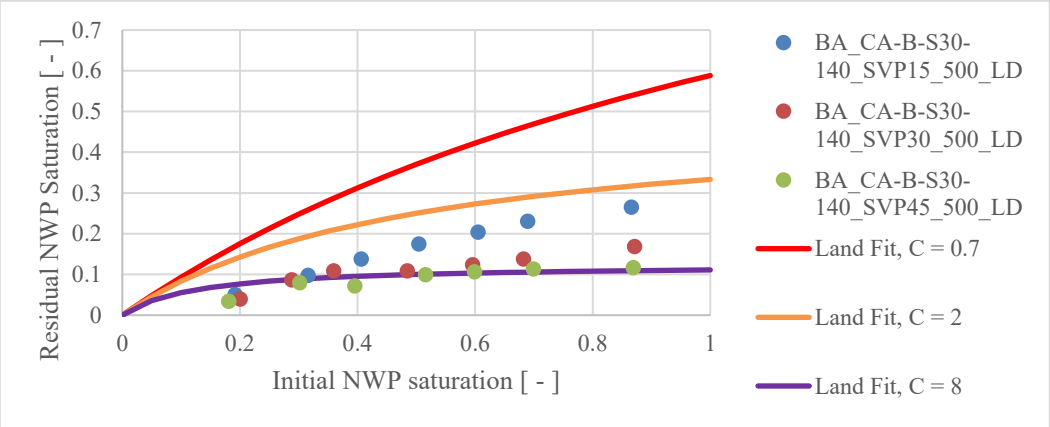

Figure 31: Reproduced trapping curves for 10° and 140° contact angles and an SVP range of 15 - 45%. (Lobel Zvonimir Danicic 2022)

4.3 Adaption in Contact Angle distribution

One of the first steps to further improve prior results in the simulation of trapping curves, the CA distribution method was upgraded from the Schultz- to the MCA-Method. The second implementation that took place simultaneously was investigating the timing of when to perform this distribution. The stochastic wettability distribution following primary drainage can significantly affect the fluid phases' behavior in the porous medium. The distribution of wettability in the medium can alter because of the preferential displacement of the non-wetting phase (NWP) from the larger pores and trapping in the smaller pores during primary drainage.

After primary drainage, if the stochastic wettability distribution is not updated, the model may be unable to effectively anticipate how the fluid phases would behave throughout subsequent drainage and imbibition operations. This is because wettability distribution can impact the

medium's relative permeability and capillary pressure curves, which are necessary to forecast the behavior of the fluid phases.

4.3.1 Change of the distribution timing

With an increase in the initial NWP saturation, there is a pronounced overlap between Figure 32, Figure 33, and Figure 34. However, the lowest regions show significant variances. The newly developed methods, which use the multiple CA and change the execution order, produce a better agreement with the benchmark simulation run on a domain size of 1000^3. A rise in the Land parameter used for assessment coincides with an increase in the SVP. When studies were run with a 15% SVP, the parameter C's lower limit for the 500^3 domain was discovered to be 4. In studies with a greater SVP of 45%, this value rises to C=8.

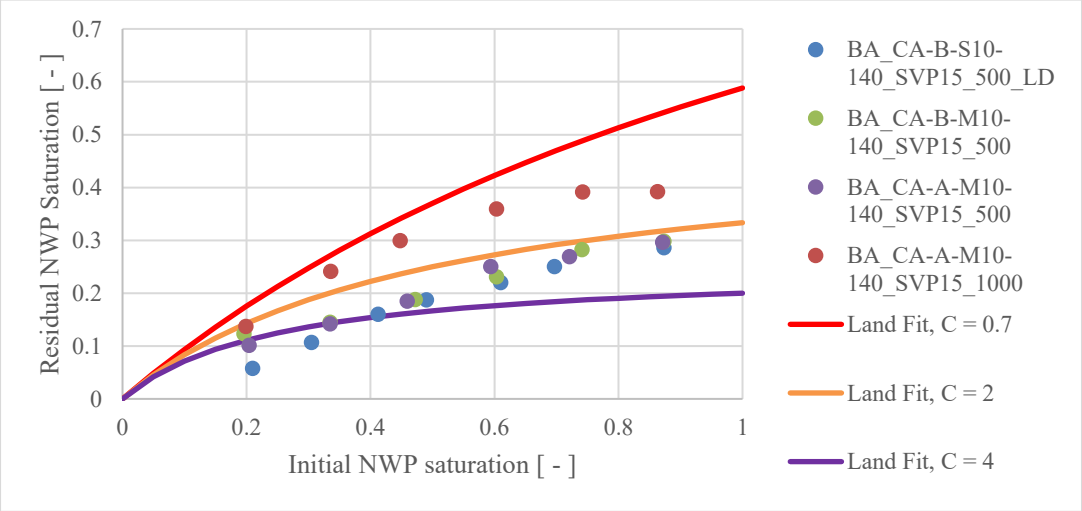

Figure 32: Simulations with MCA distribution for the 500^3 and 1000^3 domain with the distribution before and after the primary drainage for a contact angle of 10° and 140° and an SVP of 15%

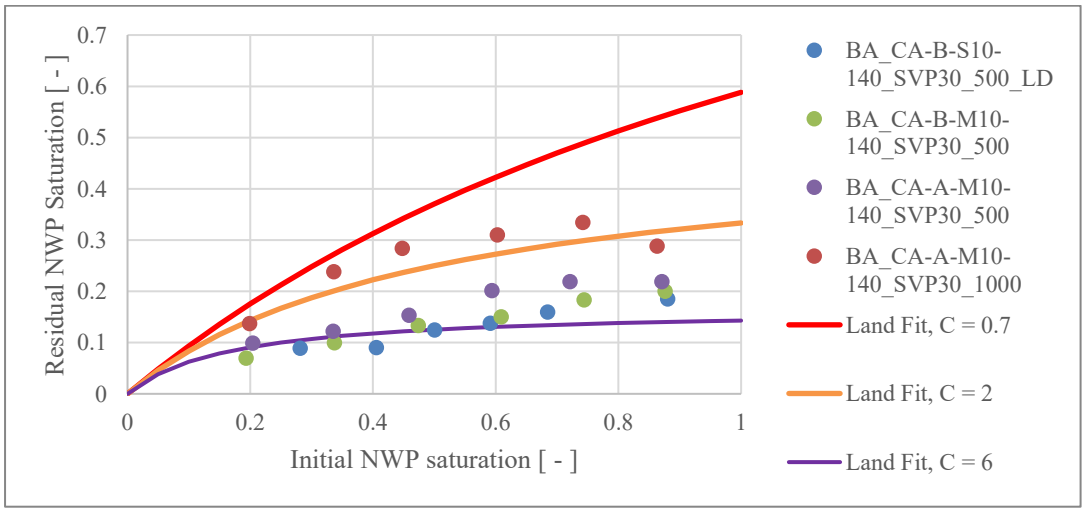

Figure 33: Simulations with MCA distribution for the 500^3 and 1000^3 domain with the distribution before and after the primary drainage for a contact angle of 10° and 140° and an SVP of 30%

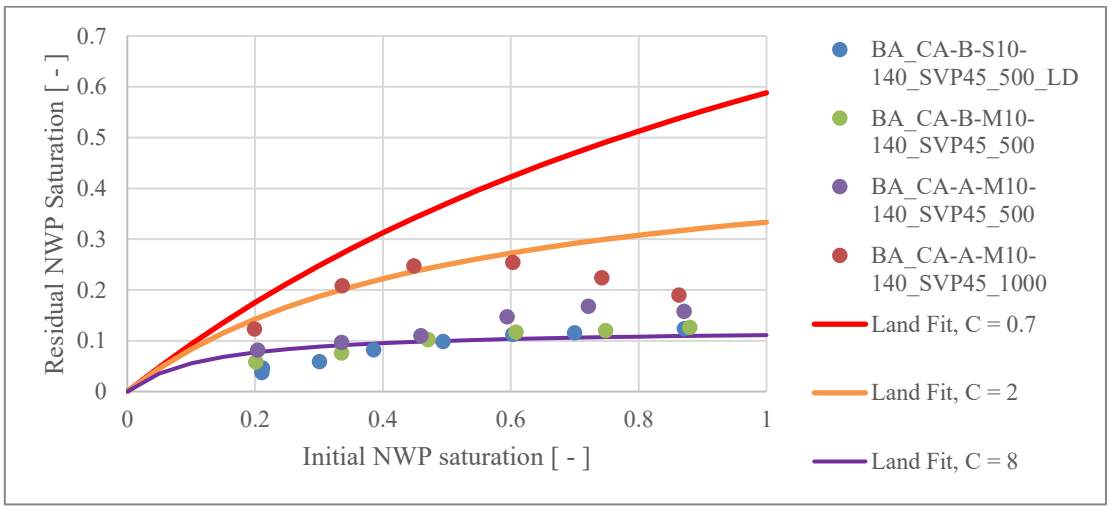

Figure 34: Simulations with MCA distribution for the 500³ and 1000³ domain with the distribution before and after the primary drainage for a contact angle of 10° and 140° and an SVP of 45%

The exact sequence of simulations was conducted on the identical rock sample, this time involving a change in contact CA to 30° and 140°. The outcome trends remain consistent with the previous experiments, as depicted in Figure 35, Figure 36, and Figure 37. However, it's important to note that compared to the experiments performed by (Lobel Zvonimir Danicic 2022), the deviation is more pronounced when the CA is increased by 10°.

As the solid volume percentage steadily increases, it becomes evident that the deviations, particularly for lower initial NWP saturations, are more inclined towards the literature values of C = 0.7 – 2 for simulations where the CA distribution occurs after primary drainage. The 10° - 140° experiments also observed a similar albeit less pronounced pattern. Consequently, for the 1000³ domain, the selected approach involved MCA distribution after primary drainage. These experiments achieved excellent alignment, especially for low SVP values.

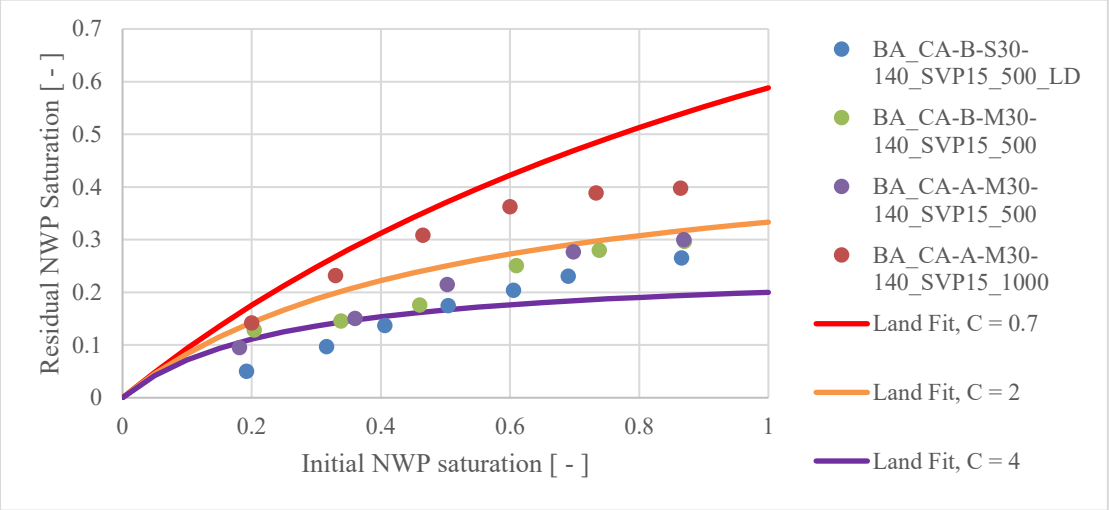

Figure 35: Comparison of the simulation approach with the MCA method for the 500³ and 1000³ domain with the distribution before and after the primary drainage for a contact angle of 30° and 140° and an SVP of 15%

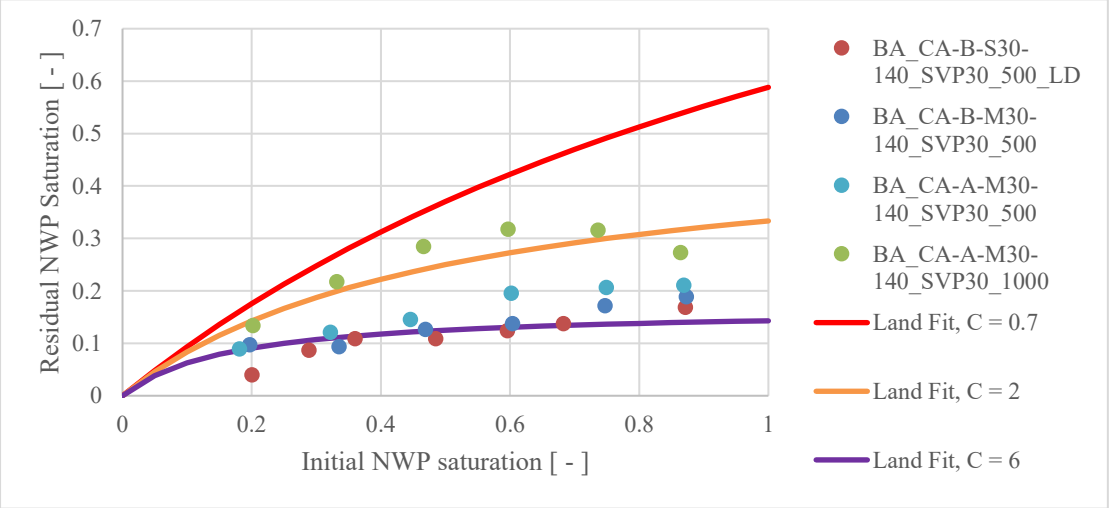

Figure 36: Comparison of the simulation approach with the MCA method for the 500³ and 1000³ domain with the distribution before and after the primary drainage for a contact angle of 30° and 140° and an SVP of 30%

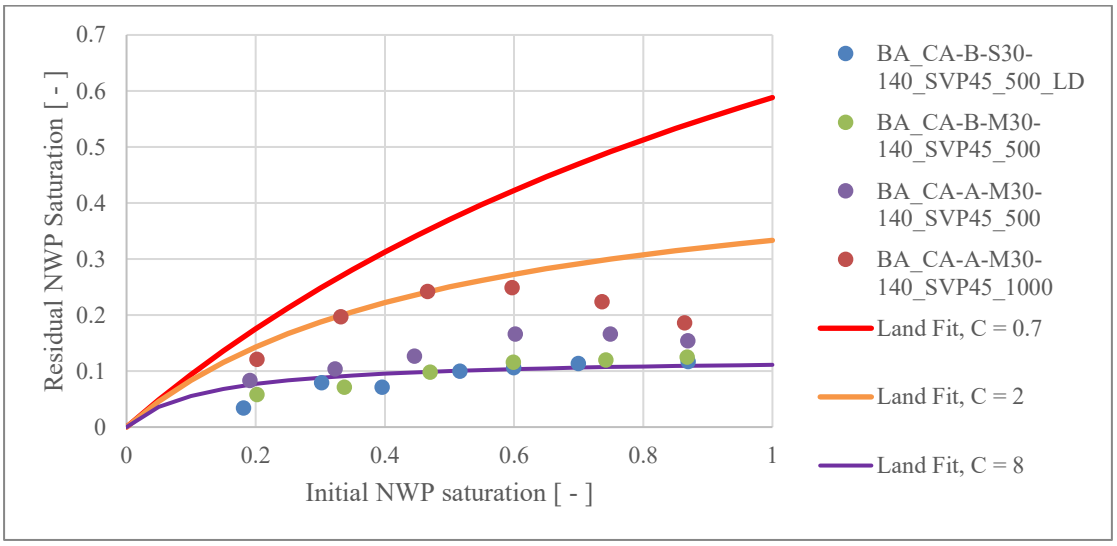

Figure 37: Comparison of the simulation approach with the MCA method for the 500³ and 1000³ domain with the distribution before and after the primary drainage for a contact angle of 30° and 140° and an SVP of 45%

Until now, the comparison between the two techniques for determining contact angle distribution has been limited to replicated strategies using the Schultz method and strategies involving the distribution after the initial drainage using the MCA method. Consequently, the subsequent phase involved contrasting the outcomes of simulations that employed the Schultz method posts the primary drainage stage. As depicted in Figure 38, the MCA methods align more closely with the projected outcomes documented in the existing literature, irrespective of when the distribution was applied.

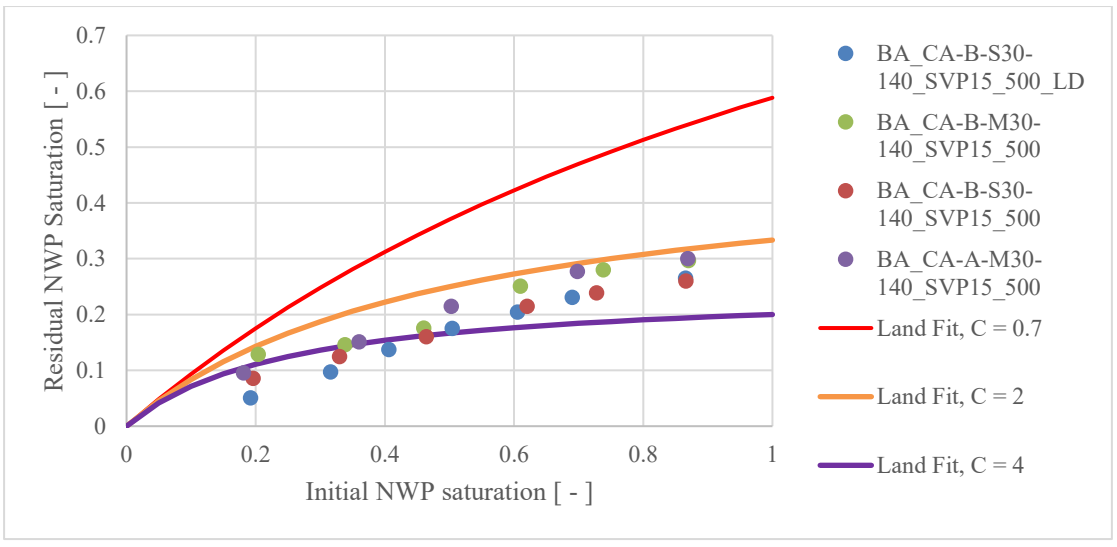

Figure 38: Comparison of the simulation approach with the MCA method for the 500³ and 1000³ domain with the distribution before and after the primary drainage for a contact angle of 30° and 140° and an SVP of 15%

The impact impact of the when the contact angle distribution was investigated in the following simulations. Figure 39 and Figure 40 show the earliest simulations focused on the trials with a 10°/140° contact angle. Figure 39 shows the simulation sequence where the contact angle distribution was conducted after the primary drainage. It has to be noted that the fit is much narrower, which means that the lower land constant is C = 5. In Figure 40, where the distribution took place after the primary drainage process, the fit is further spread out and is therefore shown with a Land factor of C = 8. Another notable difference is that although the results seem to differ less with lower SVPs, the experiment's results after the drainage process fit better in the land model.

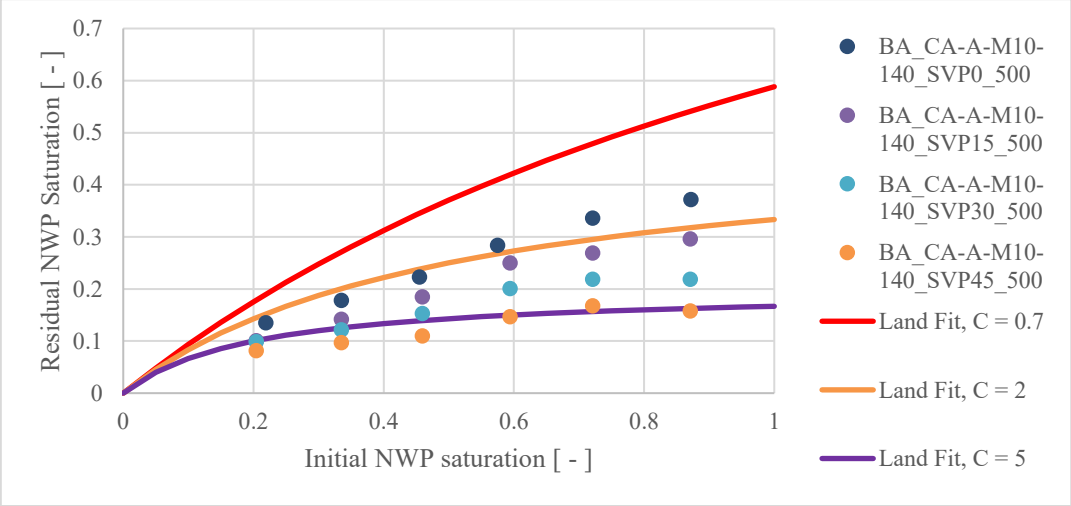

Figure 39: Visualization of the Impact of a change in Solid Volume Percentage for Simulations performed with the MCA method and the CA distribution after the primary drainage for a contact angle of 10° and 140°

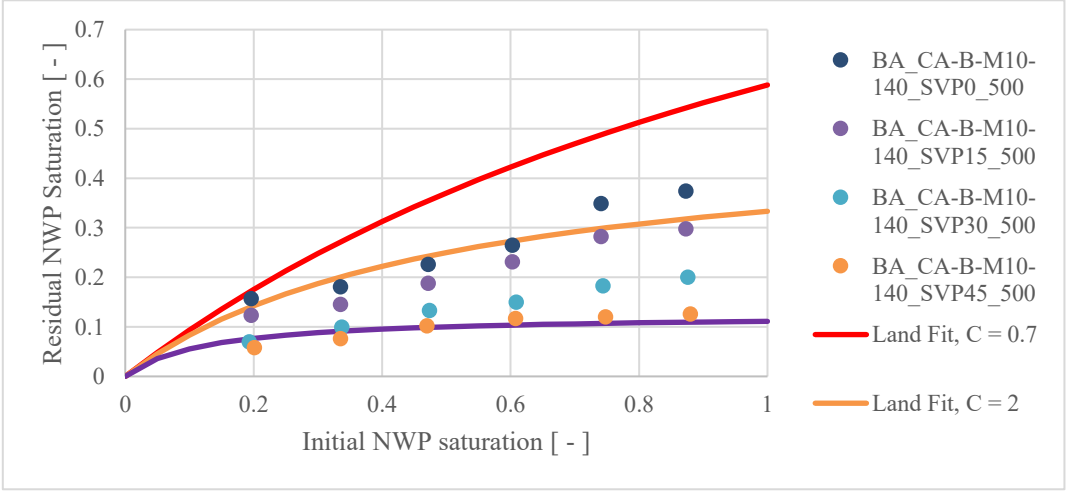

Figure 40: Visualization of the Impact of a change in Solid Volume Percentage for Simulations performed with the MCA method and the CA distribution before the primary drainage for a contact angle of 10° and 140°

Comparable outcomes can be noticed in relation to the simulations conducted with the 30°/140° configuration, as depicted in Figure 42. However, a noteworthy distinction can be identified in terms of the overall spread, which appears to be more pronounced, and the distribution, which displays a slightly more erratic pattern.

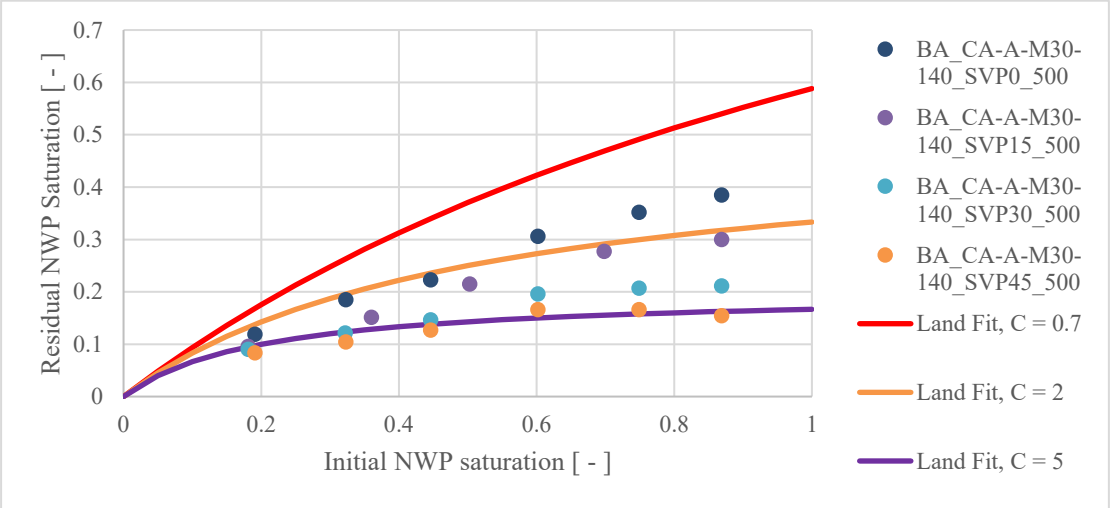

Figure 41: Visualization of the Impact of a change in Solid Volume Percentage for Simulations performed with the MCA method and the CA distribution after the primary drainage for a contact angle of 30° and 140°

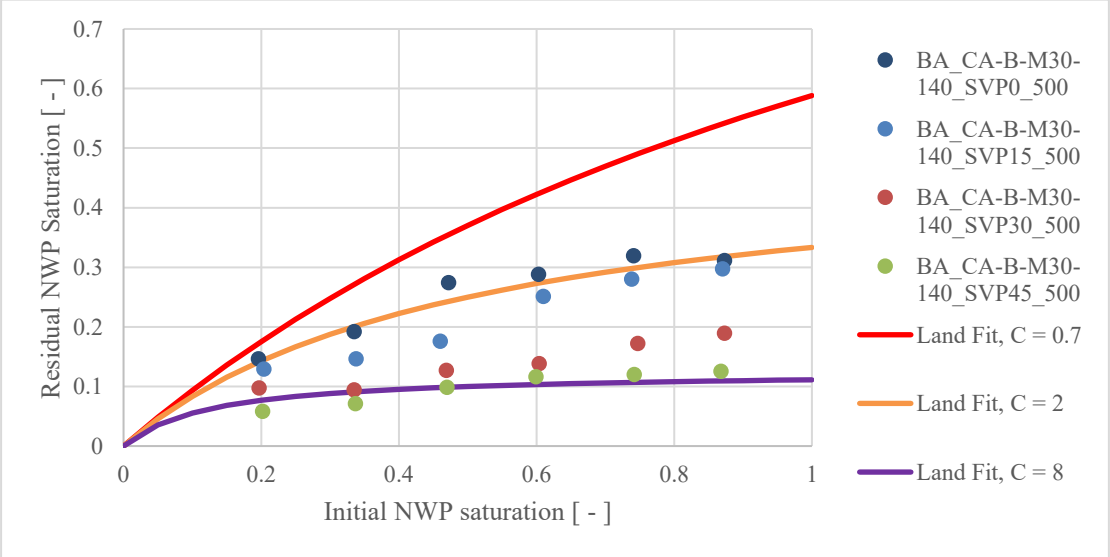

Figure 42: Visualization of the Impact of a change in Solid Volume Percentage for Simulations performed with the MCA method and the CA distribution before the primary drainage for a contact angle of 30° and 140°

4.3.2 Deterministic Distribution

This strategy comprises following a drainage phase with the application of an algorithm. The non-wetting material is primarily introduced into the larger pores where the mineral and NWP interact in this algorithm after evaluating the distribution of pore diameters. This algorithm targets the implementation of a pore volume that is considered for a change of wetting material . Because just a portion of the pore material is modified, it is crucial to understand that the volume fraction differs from the surface area fraction. The results shown in Figure 45 and Figure 46 do not show any improvement compared to the experiments conducted with the stochastic approach. Neither the use of a bigger domain nor the change in the available volume for aging led to improved results.

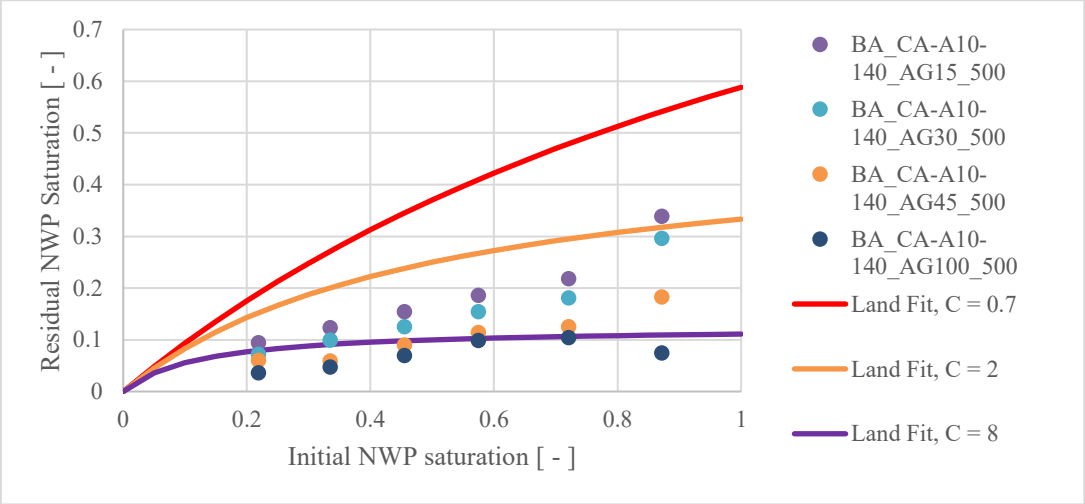

Figure 43: Visualization of the Impact of aging for Simulations performed with the MCA method and the CA distribution after the primary drainage for a contact angle of 10° and 140° and the 500³ domain.

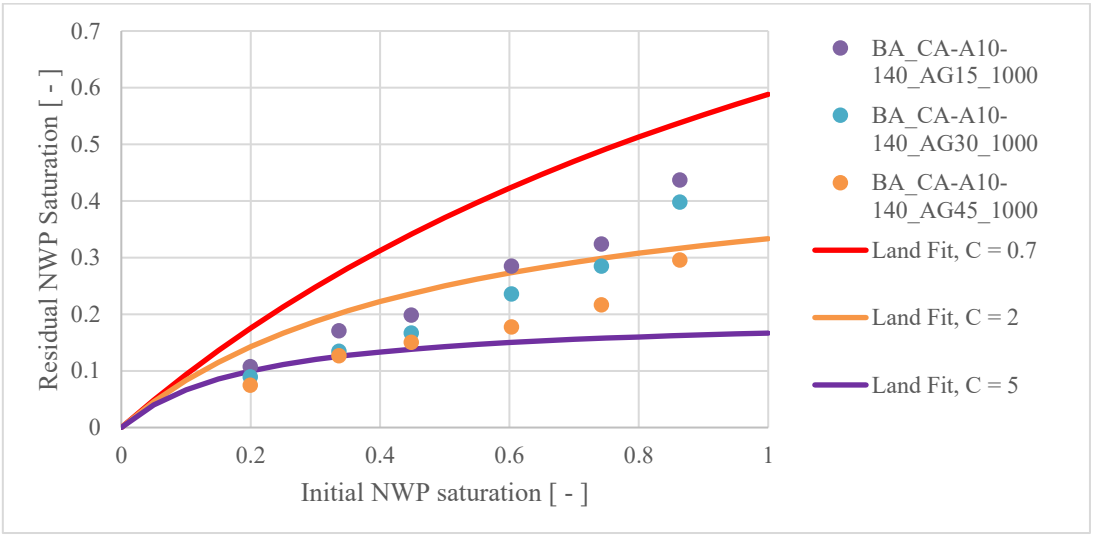

Figure 44: Visualization of the Impact of aging for Simulations performed with the MCA method and the CA distribution after the primary drainage for a contact angle of 10° and 140° and the 1000³domain.

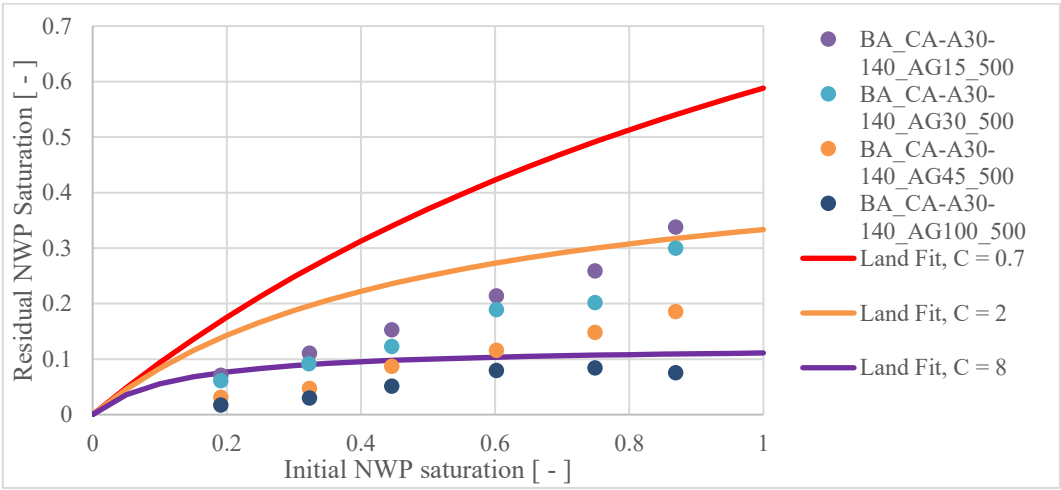

Figure 45: Visualization of the Impact of aging for Simulations performed with the MCA method and the CA distribution after the primary drainage for a contact angle of 30° and 140° and the 500³ domain.

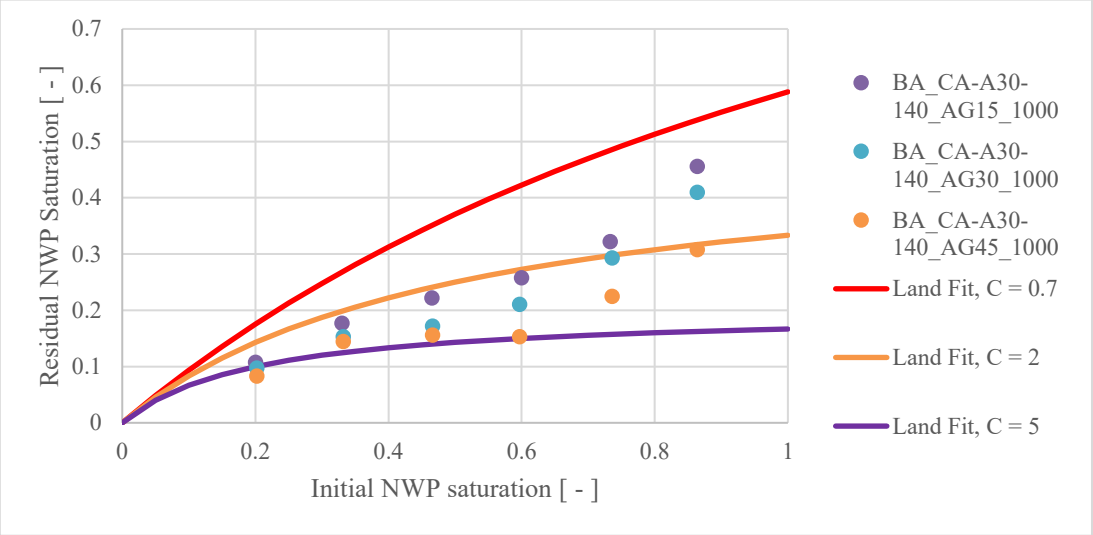

Figure 46: Visualization of the Impact of aging for Simulations performed with the MCA method and the CA distribution after the primary drainage for a contact angle of 30° and 140° and the 1000³domain.

4.3.3 Impact of the Domain Size

The next step was to further investigate different domain sizes with methodologies that showed the most promising results on a 500³ domain. To simulate the 1000³ mirroring techniques were applied to remove CCEs to help us establish the REV.

The relative orientations of the NWP and WP reservoirs are significanct in the mirrored-domain technique. The domain underwent Z-direction mirroring to analyze the potential consequences caused by boundary effects entirely. In the fully enlarged domain, imbibition and drainage processes were carried out, and the original structure and the expansive domain were used to evaluate saturations.

The invading phase starts on the Z-side during the changeover to the imbibition phase. Any boundary-end artifacts are expected to primarily appear close to the NWP reservoir located on the Z+ side. Considering this, it is suggested that all outcomes connected with the mirrored technique be examined from the Z side. Since this side relies less on NWP connection during the imbibition process, it is anticipated that it won't have strong boundary end effects, as painstakingly described in the procedure.

The findings from the analysis of the Berea structure include a comparison of the domain sizes at their original and completely expanded (mirrored) states. It becomes clear that the best trapping potential seen in simulations where when only SI (SVP=0) was employed. Even with

mirroring strategies to counteract end effects of an additional 1000³ voxel in the flow direction. This means for us that the REV was deterimned on the 1000³ voxel domain.

A pattern becomes more apparent when looking at things from a bigger picture. Most of these simulations match the the Land parameter range. The range, from C=0.7 to C=4, captures these simulations.

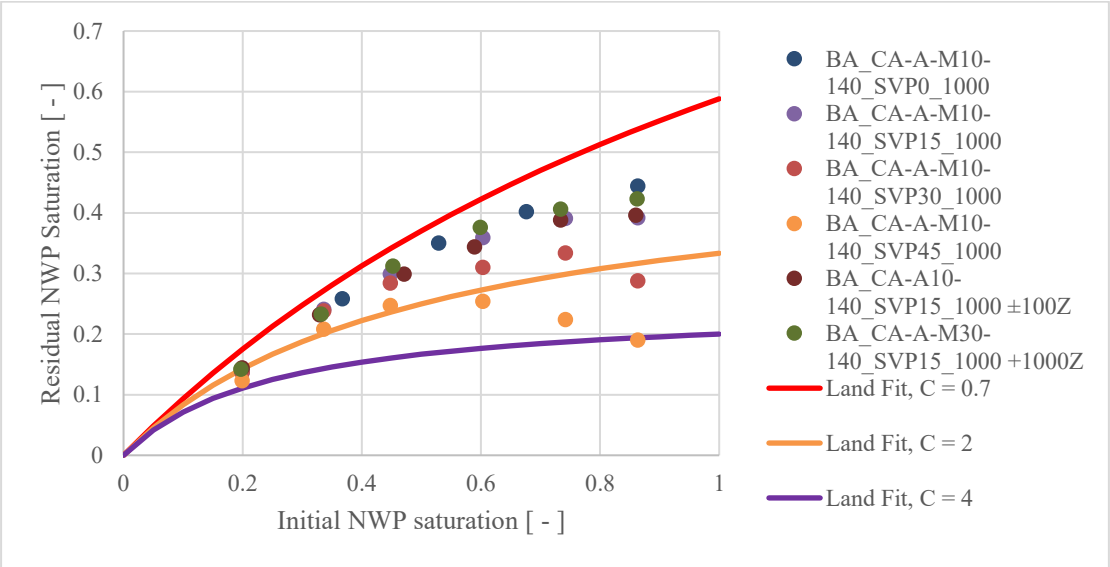

Figure 47: Visualization of the Impact of a change in Solid Volume Percentage for Simulations performed with the MCA method and the CA distribution after the primary drainage for a contact angle of 10° and 140° on a 1000³ domain.

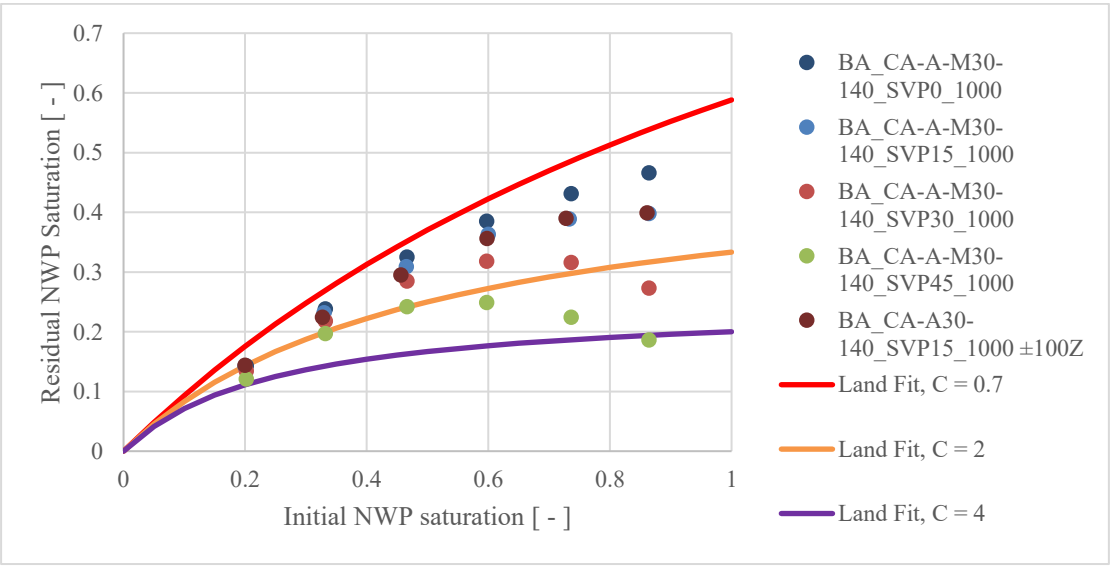

Figure 48: Visualization of the Impact of a change in Solid Volume Percentage for Simulations performed with the MCA method and the CA distribution after the primary drainage for a contact angle of 30° and 140° on a 1000³ domain.

Chapter 5

Conclusion

The main objective of this thesis is to implement a procedure that creates a benchmark for further experiments on capillary trapping potential. Previous approaches only allowed for flexibility in the applied contact angle and only modeled spontaneous imbibition. Therefore, a methodology was developed to empathize with the contribution of forced imbibition. The higher the impact of the forced imbibition, the faster the zero crossing of the capillary pressure curve and the lower the capillary trapping potential.

In order to investigate how forced imbibition affects the capillary trapping potential, the stochastic approach was explicitly used. We adopted this method to add randomness and variability to the research so that we could better understand the complex consequences of forced imbibition on trapping behavior. Numerical results were compared to experimental data from the literature. Combining this methodology and distributing contact angles after primary drainage leads to the best results. This methodology was used to determine the REV.

As a comparison, simulations with a deterministic contact angle distribution were performed. In this approach, only pores which are in contact with the NWPare taken into consideration, where bigger pores are preferred. Compared to simulations using the stochastic approach, the results do not demonstrate any improvement, even when simulating on larger domains.

In the beginning only simulations on a 500^3 voxels domain were performed. It was later shown, that this domain was too small to gather meaningful results. However, behavioral trends could be observed and a smaller domain size might be considered for future simulations to save on computational time and visualize trends. Therefore, simulations on larger domains were performed. This helped us determine the REV as well as to mitigate CEE. It was observed that results did show none or only minor changes for domains greater 1000^3. Which leads to the conclusion that a domain of 1000^3 is sufficient to analyze the trapping potential and displays our REV.

While comparing the different 10°-140° and the 30°-140° CA variation, we observeed that an increase of the CA on the wetting material leads to a decrease in trapping potential. The changed sequence, where the distribution is applied after primary drainage, impacts the trapping curve and correlates results closer to the ones of the literature.

This study made it possible to predict the capillary trapping potential of reservoir rocks to be performed precisely and on time. This helps to understand the trapping of CO_2 within the pores of the geological reservoir rock to ensure the long-term safety and integrity of CO_2 storage sites.

5.1 Future Work

Even though the smaller (500^3 voxels) domain quickly produced reliable trends, it is crucial to examine the heterogeneity aspect when comparing it to the larger (1000^3 voxels) domains. It is vital to understand that the smaller domain is a subset cropped from the bigger domain's center region and not simply a scaled-down reproduction of the larger domain. Therefore, other areas than the core must be tested for their potential, and possible correlations to pore structures can be made.

The approaches used to study the 1000^3 domains provided a preliminary understanding of the capillary trapping capability of the Berea sandstone. It is essential to broaden these approaches to include a broader range of sandstones and expand the inquiry to carbonate reservoirs due to the restriction to a particular rock type. The applicability and dependability of these methods in many scenarios will be established with the aid of this expansion.

Lastly, the subsequent logical progression involves a direct comparison to laboratory experiments, substantiating the validity of simulation outcomes and emphasizing their relevance in advancing CCS projects.

List of Figures

Nomenclature

m	mass	[kg]
r	radius	[m]
P_c	capillary pressure	[Pa]
θ	contact angle	[°]
σ	interfacial tension	[N/m]
C	Land-model parameter	[-]

Abbreviations

capillary end effect
CEE 31
Carbon Capture and Storage
CCS vii
Carbonated Water
CW 22
Carbonated Water Injection
CWI 20
Contact Angle
CA 54
Digital Rock Physics
DRP vii
Enhanced Oil Recovery
EOR 22
Forced imbibition
FI
Initial-Residual
IR 32
Interfacial Tension
IFT .....
Morphological Method
MM 14
Multiple Contact Angle
MCA 59
Non-Wetting Phase
NWP 14
Representative Elementary Volume
REV 30
Simultaneous Water and Gas injection
SWAG 21
Solid Volume Percentage
SVP 44
Special Core Analysis
SCAL vii
Spontaneous Imbibition
SI
Super Critical
SC 20
Water Alternating Gas injection
WAG 21

References

Abbaszadeh, Mohsen; Shariatipour, Seyed; Ifelebuegu, Augustine (2020): The influence of temperature on wettability alteration during CO2 storage in saline aquifers. In *International Journal of Greenhouse Gas Control* 99, p. 103101. DOI: 10.1016/j.ijggc.2020.103101.

Ajayi, Temitope; Gomes, Jorge Salgado; Bera, Achinta (2019): A review of CO2 storage in geological formations emphasizing modeling, monitoring and capacity estimation approaches. In *Pet. Sci.* 16 (5), pp. 1028–1063. DOI: 10.1007/s12182-019-0340-8.

Alcorn, Zachary Paul; Føyen, Tore; Zhang, Leilei; Karakas, Metin; Biswal, Sibani Lisa; Hirasaki, George; Graue, Arne (2020): CO2 Foam Field Pilot Design and Initial Results. In : Day 1 Mon, August 31, 2020. SPE Improved Oil Recovery Conference. Virtual, 31/08/2020 - 04/09/2020: SPE.

Alexander, Lisa V. (2016): Global observed long-term changes in temperature and precipitation extremes: A review of progress and limitations in IPCC assessments and beyond. In *Weather and Climate Extremes* 11, pp. 4–16. DOI: 10.1016/j.wace.2015.10.007.

Alexandru-Mihai Badescu (2020): Digital Rock Physics for Unconsolidated Sandstones–A Grain Size Distribution Approach. Available online at https://pureadmin.unileoben.ac.at/ws/files/6086694/ac16128890.pdf.

Al-Menhali, Ali; Krevor, Samuel (2014): Effective Wettability Measurements of CO2-brine-Sandstone System at Different Reservoir Conditions. In *Energy Procedia* 63, pp. 5420–5426. DOI: 10.1016/j.egypro.2014.11.572.

Al-Menhali, Ali S.; Krevor, Samuel (2016): Capillary Trapping of CO2 in Oil Reservoirs: Observations in a Mixed-Wet Carbonate Rock. In *Environmental science & technology* 50 (5), pp. 2727–2734. DOI: 10.1021/acs.est.5b05925.

Arnold, Pit (2018): Experimental investigation of interfacial tension for alkaline flooding.

Arnold, Pit; Dragovits, Mario; Linden, Sven; Hinz, Christian; Ott, Holger (2023): Forced imbibition and uncertainty modeling using the morphological method. In *Advances in Water Resources* 172, p. 104381. DOI: 10.1016/j.advwatres.2023.104381.

Bakke, Stig; Øren, Pål-Eric (1997): 3-D Pore-Scale Modelling of Sandstones and Flow Simulations in the Pore Networks. In *SPE Journal* 2 (02), pp. 136–149. DOI: 10.2118/35479-PA.

Bear, Jacob; Bachmat, Yehuda (1998): Introduction to modeling of transport phenomena in porous media. [Repr.]. Dordrecht: Kluwer (Theory and applications of transport in porous media, vol. 4).

Benson, S. M.; Cole, D. R. (2008): CO2 Sequestration in Deep Sedimentary Formations. In *Elements* 4 (5), pp. 325–331. DOI: 10.2113/gselements.4.5.325.

Blunt, Martin J. (2017): Multiphase Flow in Permeable Media: Cambridge University Press.

Brown, G. O.; Hsieh, H. T.; Lucero, D. A. (2000): Evaluation of laboratory dolomite core sample size using representative elementary volume concepts. In *Water Resour. Res.* 36 (5), pp. 1199–1207. DOI: 10.1029/2000WR900017.

Bryant, Steven L.; Mellor, David W.; Cade, Christopher A. (1993): Physically representative network models of transport in porous media. In *AIChE J.* 39 (3), pp. 387–396. DOI: 10.1002/aic.690390303.

C. Marchetti (1977): On Geoengineering and the CO2 problem. In *Climate Change* 1, pp. 59–68.

Cao, Yan; Seyed Alizadeh, Seyed Mehdi; Fouladvand, Mohammad Taghi; Khan, Afrasyab; Taghvaie Nakhjiri, Ali; Heidari, Zahra et al. (2021): Mathematical modeling and numerical simulation of CO2 capture using MDEA-based nanofluids in nanostructure membranes. In *Process Safety and Environmental Protection* 148, pp. 1377–1385. DOI: 10.1016/j.psep.2021.03.007.

Carlon S. Land (1968): Calculation of Imbibition Relative Permeability for Two- and Three-Phase Flow From Rock Properties. In *Society of Petroleum Engineers Journal* 8, pp. 149–156.

Celia, M. A.; Bachu, S.; Nordbotten, J. M.; Bandilla, K. W. (2015): Status of CO 2 storage in deep saline aquifers with emphasis on modeling approaches and practical simulations. In *Water Resour. Res.* 51 (9), pp. 6846–6892. DOI: 10.1002/2015WR017609.

Dvorkin; Armbruster; Baldwin; Fang; Derzhi; Gomez et al. (2008): The future of rock physics: computational methods vs. lab testing. In *First Break* 26, pp. 63–68.

Elizabeth J. Spiteri; Ruben Juanes; Martin J. Blunt; Franklin M. Orr, JR. (2008): A New Model of Trapping and Relative Permeability Hysteresis for All Wettability Characteristics. In *Society of Petroleum Engineers Journal* 13, pp. 277–288.

Eric H. Oelkers; Sigurour R. Gislason; Sandra O.; Bergur Sigfusson; Chiara Marieni; David Goldberg (2020): Mineral Storage of CO2.

Esene, Cleverson; Rezaei, Nima; Aborig, Amer; Zendehboudi, Sohrab (2019): Comprehensive review of carbonated water injection for enhanced oil recovery. In *Fuel* 237, pp. 1086–1107. DOI: 10.1016/j.fuel.2018.08.106.

Farokhpoor, Raheleh; Bjørkvik, Bård J.A.; Lindeberg, Erik; Torsæter, Ole (2013): Wettability behaviour of CO2 at storage conditions. In *International Journal of Greenhouse Gas Control* 12, pp. 18–25. DOI: 10.1016/j.ijggc.2012.11.003.

Georges Matheron; Jean Serra (1998): The birth of Mathematical Morphology.

Hadley, G. F.; Handy, L. L.: A Theoretical and Experimental Study of the Steady State Capillary End Effect. In : 1956.

Hassanzadeh, Hassan; Pooladi-Darvish, Mehran; Keith, David W. (2009): Accelerating CO 2 Dissolution in Saline Aquifers for Geological Storage — Mechanistic and Sensitivity Studies. In *Energy Fuels* 23 (6), pp. 3328–3336. DOI: 10.1021/ef900125m.

Hepple, R. P.; Benson, S. M. (2005): Geologic storage of carbon dioxide as a climate change mitigation strategy: performance requirements and the implications of surface seepage. In *Environ Geol* 47 (4), pp. 576–585. DOI: 10.1007/s00254-004-1181-2.

Hilpert, Markus; Miller, Cass T. (2001): Pore-morphology-based simulation of drainage in totally wetting porous media. In *Advances in Water Resources* 24 (3-4), pp. 243–255. DOI: 10.1016/S0309-1708(00)00056-7.

Hui, Mun-Hong; Blunt, Martin J. (2000): Effects of Wettability on Three-Phase Flow in Porous Media. In *J. Phys. Chem. B* 104 (16), pp. 3833–3845. DOI: 10.1021/jp9933222.

IOGP Publications library (2023): Map of global CCUS projects | IOGP Publications library. Available online at https://www.iogp.org/bookstore/product/map-of-global-ccs-projects/, updated on 8/7/2023, checked on 8/7/2023.

IPCC special report on carbon dioxide capture and storage (2005). Available online at https://repository.ubn.ru.nl/bitstream/handle/2066/230961/230961.pdf?sequence=1.

Jayasekara, D. W.; Ranjith, P. G.; Wanniarachchi, W.A.M.; Rathnaweera, T. D. (2020): Understanding the chemico-mineralogical changes of caprock sealing in deep saline CO2 sequestration environments: A review study. In *The Journal of Supercritical Fluids* 161, p. 104819. DOI: 10.1016/j.supflu.2020.104819.

Juanes, R.; Spiteri, E. J.; Orr, F. M.; Blunt, M. J. (2006): Impact of relative permeability hysteresis on geological CO 2 storage. In *Water Resour. Res.* 42 (12). DOI: 10.1029/2005WR004806.

Killough, J. E. (1976): Reservoir Simulation With History-Dependent Saturation Functions. In *Society of Petroleum Engineers Journal* 16 (01), pp. 37–48. DOI: 10.2118/5106-PA.

Krevor, Samuel; Blunt, Martin J.; Benson, Sally M.; Pentland, Christopher H.; Reynolds, Catriona; Al-Menhali, Ali; Niu, Ben (2015): Capillary trapping for geologic carbon dioxide storage – From pore scale physics to field scale implications. In *International Journal of Greenhouse Gas Control* 40, pp. 221–237. DOI: 10.1016/j.ijggc.2015.04.006.

L. Nghiem; V. Shrivastava; B. Kohse; M. Hassam; C. Yang; Computer Modelling Group Ltd.:])Qqq{Simulation and Optimization of Trapping Processes for CO2 Storage in Saline Aquifers.

Lamy, Celine; Iglauer, Stefan; Pentland, Christopher H.; Blunt, Martin J.; Maitland, Geoffrey (2010): Capillary Trapping in Carbonate Rocks. In : All Days. SPE EUROPEC/EAGE Annual Conference and Exhibition. Barcelona, Spain, 14/06/2010 - 17/06/2010: SPE.

Larsen, J. A.; Skauge, Arne (1998): Methodology for Numerical Simulation With Cycle-Dependent Relative Permeabilities. In *SPE Journal* 3 (02), pp. 163–173. DOI: 10.2118/38456-PA.

Liao, Jianxing; Cao, Cheng; Hou, Zhengmeng; Mehmood, Faisal; Feng, Wentao; Yue, Ye; Liu, Hejuan (2020): Field scale numerical modeling of heat extraction in geothermal reservoir based on fracture network creation with supercritical CO2 as working fluid. In *Environ Earth Sci* 79 (12). DOI: 10.1007/s12665-020-09001-7.

Lobel Zvonimir Danicic (2022): Sensitivity Analysis of the Trapping Potential of Different Rock Types using Digital Rock Physics. Available online at https://pureadmin.unileoben.ac.at/ws/files/8805005/ac16505951.pdf.

Lyu, Xiaocong; Voskov, Denis; Rossen, William R. (2021): Numerical investigations of foam-assisted CO2 storage in saline aquifers. In *International Journal of Greenhouse Gas Control* 108, p. 103314. DOI: 10.1016/j.ijggc.2021.103314.

Mario Dragovits (2021): Sensitivity of capillarity on spatial wettability variation: Application of a modified morphological approach. Available online at https://pure.unileoben.ac.at/en/publications/sensitivity-of-capillarity-on-spatial-wettability-variation-appli.

Martin Blunt; Michael J. King; and Harvey Scher (1992): Simulation and theory of two-phase flow in porous media. In *Physical Review A* 46, pp. 7680–7699.

Mohammad Derakshanfar (2012): Effects on waterflooding, solvent injection, and solvent convective dispersion on vapour extraction (vapex) heavy oil recovery.

Motie, Mohadeseh; Assareh, Mehdi (2020): CO2 sequestration using carbonated water injection in depleted naturally fractured reservoirs: A simulation study. In *International Journal of Greenhouse Gas Control* 93, p. 102893. DOI: 10.1016/j.ijggc.2019.102893.

Ott, Holger; Oedai, Sjaam (2015): Wormhole formation and compact dissolution in single- and two-phase CO 2 -brine injections. In *Geophys. Res. Lett.* 42 (7), pp. 2270–2276. DOI: 10.1002/2015GL063582.

Raza, Arshad; Gholami, Raoof; Rezaee, Reza; Rasouli, Vamegh; Rabiei, Minou (2019): Significant aspects of carbon capture and storage – A review. In *Petroleum* 5 (4), pp. 335–340. DOI: 10.1016/j.petlm.2018.12.007.

Raza, Arshad; Rezaee, Reza; Bing, Chua Han; Gholami, Raoof; Hamid, Mohamed Ali; Nagarajan, Ramasamy (2016): Carbon dioxide storage in subsurface geologic medium: A review on capillary trapping mechanism. In *Egyptian Journal of Petroleum* 25 (3), pp. 367–373. DOI: 10.1016/j.ejpe.2015.08.002.

S. BACHU; J. SHAW (2004): Evaluation of the CO2 Sequestration Capacity in Alberta's Oil and Gas Reservoirs at Depletion and the Effect of Underlying Aquifers, pp. 1–77.

Saadatpoor, Ehsan; Bryant, Steven L.; Sepehrnoori, Kamy (2010): New Trapping Mechanism in Carbon Sequestration. In *Transp Porous Med* 82 (1), pp. 3–17. DOI: 10.1007/s11242-009-9446-6.

Sandra Ó. Snæbjörnsdóttir; Bergur Sigfússon; Chiara Marieni; David Goldberg; Sigurður R. Gislason; Eric H. Oelkers (2020): Mineral Storage of CO2.

Saraji, Soheil; Goual, Lamia; Piri, Mohammad; Plancher, Henry (2013): Wettability of supercritical carbon dioxide/water/quartz systems: simultaneous measurement of contact angle and interfacial tension at reservoir conditions. In *Langmuir : the ACS journal of surfaces and colloids* 29 (23), pp. 6856–6866. DOI: 10.1021/la3050863.

Saraji, Soheil; Piri, Mohammad; Goual, Lamia (2014): The effects of SO2 contamination, brine salinity, pressure, and temperature on dynamic contact angles and interfacial tension of supercritical CO2/brine/quartz systems. In *International Journal of Greenhouse Gas Control* 28, pp. 147–155. DOI: 10.1016/j.ijggc.2014.06.024.

Schulz, Volker P.; Wargo, Eric A.; Kumbur, Emin C. (2015): Pore-Morphology-Based Simulation of Drainage in Porous Media Featuring a Locally Variable Contact Angle. In *Transp Porous Med* 107 (1), pp. 13–25. DOI: 10.1007/s11242-014-0422-4.

Shariatipour, Seyed M.; Mackay, Eric J.; Pickup, Gillian E. (2016): An engineering solution for CO 2 injection in saline aquifers. In *International Journal of Greenhouse Gas Control* 53, pp. 98–105. DOI: 10.1016/j.ijggc.2016.06.006.

Sigurdur R.; Gislason and Eric H. Oelkers (2014): Carbon Storage in Basalt.

Stephen A. Rackley (Ed.) (2017): Carbon Capture and Storage: Elsevier.

Yu; Wardlaw (1985): Mechanisms of Nonwetting Phase Trapping during Imbibiton at Slow Rates. In *Journal of Colloid and Interface Science* 109, pp. 473–486.

Zhang, Dongxiao; Song, Juan (2014): Mechanisms for Geological Carbon Sequestration. In *Procedia IUTAM* 10, pp. 319–327. DOI: 10.1016/j.piutam.2014.01.027.